Bioorganic Chemistry 109 (2021) 104695

Contents lists available at ScienceDirect

Bioorganic Chemistry

journal homepage: www.elsevier.com/locate/bioorg

Design, synthesis and molecular modeling of new quinazolin-4(3*H*)-one based VEGFR-2 kinase inhibitors for potential anticancer evaluation

Abdallah E. Abdallah [a,*], Sally I. Eissa [b,c], Maged Mohammed Saleh Al Ward [a], Reda R. Mabrouk [a], Ahmed B.M. Mehany [d], Mohamed Ayman El-Zahabi [a,*]

[a] *Pharmaceutical Medicinal Chemistry & Drug Design Department, Faculty of Pharmacy (Boys), Al-Azhar University, Cairo 11884, Egypt*
[b] *Department of Pharmaceutical Chemistry, Faculty of Pharmacy (Girls), Al-Azhar University, Cairo 11884, Egypt*
[c] *Faculty of Pharmacy Al-Maareffa University for Science and Technology, Riyadh, Saudi Arabia*
[d] *Zoology Department, Faculty of Science, Al-Azhar University, Cairo 11884, Egypt*

ARTICLE INFO

Keywords:
Anticancer
Molecular docking
Quinazolin-4(3*H*)-one
VEGFR-2 kinase

ABSTRACT

Globally cancer is the second leading cause of death. So that this work is an attempt to develop new effective anti-cancer agents. In line with pharmacophoric features of VEGFR-2 kinase inhibitors, new nineteen quinazolin-4-one derivatives were designed, synthesized and biologically evaluated for their potential anticancer activity. All target compounds were evaluated *in vitro* for VEGFR-2 tyrosine kinase inhibition. Then, nine compounds of best results were further investigated by *in vitro* assay against three human cancer cell lines, namely HepG2, PC3 and MCF. *N*'-{2-](3-Ethyl-6-nitro-4-oxo-3,4-dihydroquinazoline-2-yl)thio[acetyl}benzohydrazide (**36**) was found to be the most potent candidate as it showed $IC_{50} = 4.6 \pm 0.06$ μM against VEGFR-2 kinase. It also exhibited $IC_{50} = 17.23 \pm 1.5$, 26.10 ± 2.2 and 30.85 ± 2.3 μg/mL against HepG2, PC3 and MCF, respectively. At the same time it showed $IC_{50} = 145.93 \pm 1.1$ μg/mL against the normal human lung fibroblasts cell line (WI-38), indicating good selectivity index. Further investigation into HepG2 cell cycle showed the ability of compound **36** to induce apoptosis and arrest cell growth at G2/M phase. Moreover, docking studies demonstrated the ability of compound 36 to bind VEGFR-2 in a correct manner making three essential hydrogen bonds with the key residues Glu885, Asp1046 and Cys919. In sum, this work suggests that compound **36** can serve as a lead for development of effective anticancer agents targeting VEGFR-2.

1. Introduction

Cancer is a worldwide major health problem. One of six death is attributed to cancer. In U.S. 1,806,590 new cancer cases and 606,520 cancer deaths are the projected numbers to occur in 2020 [1]. So that development of new anticancer agents is a global requirement to improve the current situation.

To find an effective and safe anticancer agents, the characteristics of cancer cells should be considered. Among which is secretion of growth factors. One of which vascular endothelial growth factors (VEGFs) which play a pivotal role in angiogenesis [2]. Angiogenesis is essential to supply the cancer cells with oxygen and nutrients required for growth [3]. It is also a potential cause for cancer progression and metastasis [3]. Inhibition of angiogenesis is reported as effective approach to cancer treatment [4]. It can be achieved by vascular endothelial growth factor receptors inhibition [5].

VEGFRs can be divided into three types VEGFR-1, VEGFR-2 and VEGFR-3. VEGFR-2 is the most important and takes on a pivotal role in angiogenesis process [6,7]. In comparison with normal vascular endothelial cells, neo vascular tumor endothelial cells have extensive expression of VEGFR-2 [8]. VEGFR-2 signaling pathway was shown in many cancer types for example colorectal [9], breast [10], lung non-small cell [11], urothelial [12] carcinoma. These facts drew a particular attention to inhibition of VEGFR-2 as a significant approach in treatment of cancer. Examples for FDA approved anticancer drugs that showed VEGFR-2 inhibition are pazopanib **1** [13], regorafenib **2** [14], suntinib **3** [15], sorafenib **4** [16] and vatalanib **5** [17] and Tivozanib **6** [18] (**Fig. 1**).

VEGFR-2 Kinase inhibitors can be classed into two main types [19]. Type I inhibitors e.g. sunitinib [18] occupy the region which originally occupied by ATP adenine moiety. They identify the active conformation of the receptor [20]. While type II kinase inhibitors e.g. sorafenib,

* Corresponding authors.
E-mail addresses: Abdulla_emara@azhar.edu.eg (A.E. Abdallah), Abelal_81@azhar.edu.eg (A.B.M. Mehany), malzahaby@azhar.edu.eg (M.A. El-Zahabi).

https://doi.org/10.1016/j.bioorg.2021.104695
Received 2 November 2020; Received in revised form 26 December 2020; Accepted 24 January 2021
Available online 8 February 2021

regorafenib and tivozanib [18] stabilize the inactive conformation (DFG-out) of the receptor which is formed by movement of the DFG motif (Aspartate- Phenylalanine- Glycine motif). Type II inhibitors primarily occupy an allosteric site which is a hydrophobic and appears directly adjacent to the ATP binding domain. This allosteric site is emerged only in the inactive conformation of the enzyme [21]. Type-II kinase inhibitors are better than type-I inhibitors due to improved kinase selectivity and slower off-rates [22].

Quinazoline nucleus was used as a scaffold for development of potent anticancer agents targeting VEGFR-2 [23,24]. One of quinazoline containing compounds is the potent VEGFR-2 inhibitor AZD-2932 **7** (Fig. 1) [25].

1.1. Rationale of drug design.

The design was mainly based on the common essential pharmacophoric features of type II VEGFR-2 kinase inhibitors as illustrated in Fig. 2. Four features have been identified [26,27]; 1- flat hetero aromatic moiety which occupies ATP binding domain and forms hydrogen bonds with the key residues Cys919 and/or Glu917 [28,18]. 2-aryl linker which occupies the area between ATP binding domain and DFG domain [29]. 3- hydrogen bond acceptors and donors which forms hydrogen bonds with the key residues Glu885 and Asp1046 in the DFG domain [28]. 4- terminal hydrophobic moiety which binds via hydrophobic interactions to the created hydrophobic allosteric pocket [28]. This pocket is revealed when the phenylalanine residue of the DFG loop of the enzyme flips out of its lipophilic pocket presenting DFG-out or inactive conformation [30].

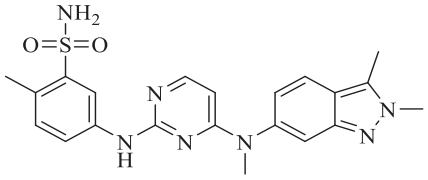

Pazopanib **1**

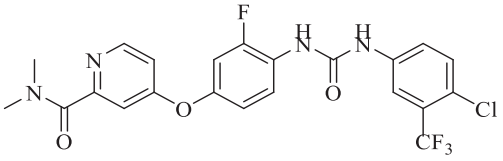

Regorafenib **2**

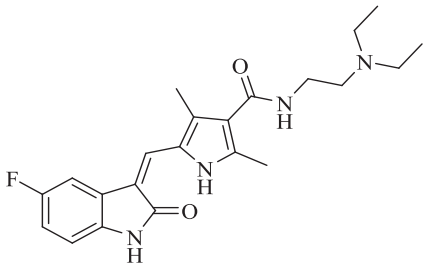

Sunitinib **3**

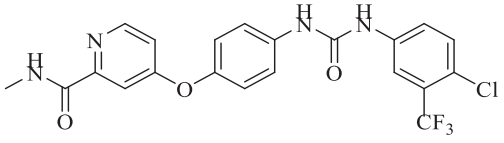

Sorafenib **4**

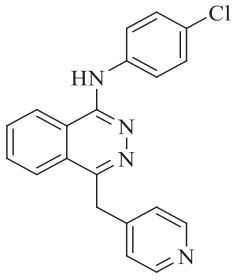

Vatalanib **5**

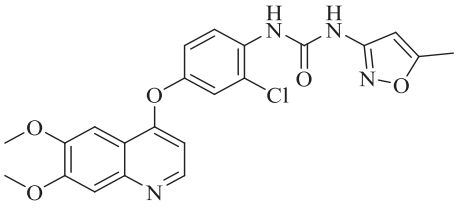

Tivozanib **6**

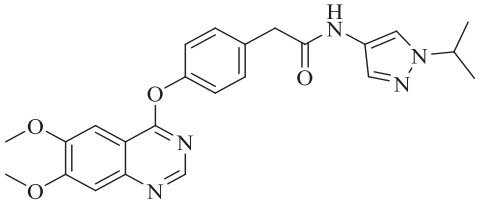

AZD-2932 **7**

Fig. 1. Chemical structures of some currently approved VEGFR-2 kinase inhibitors.

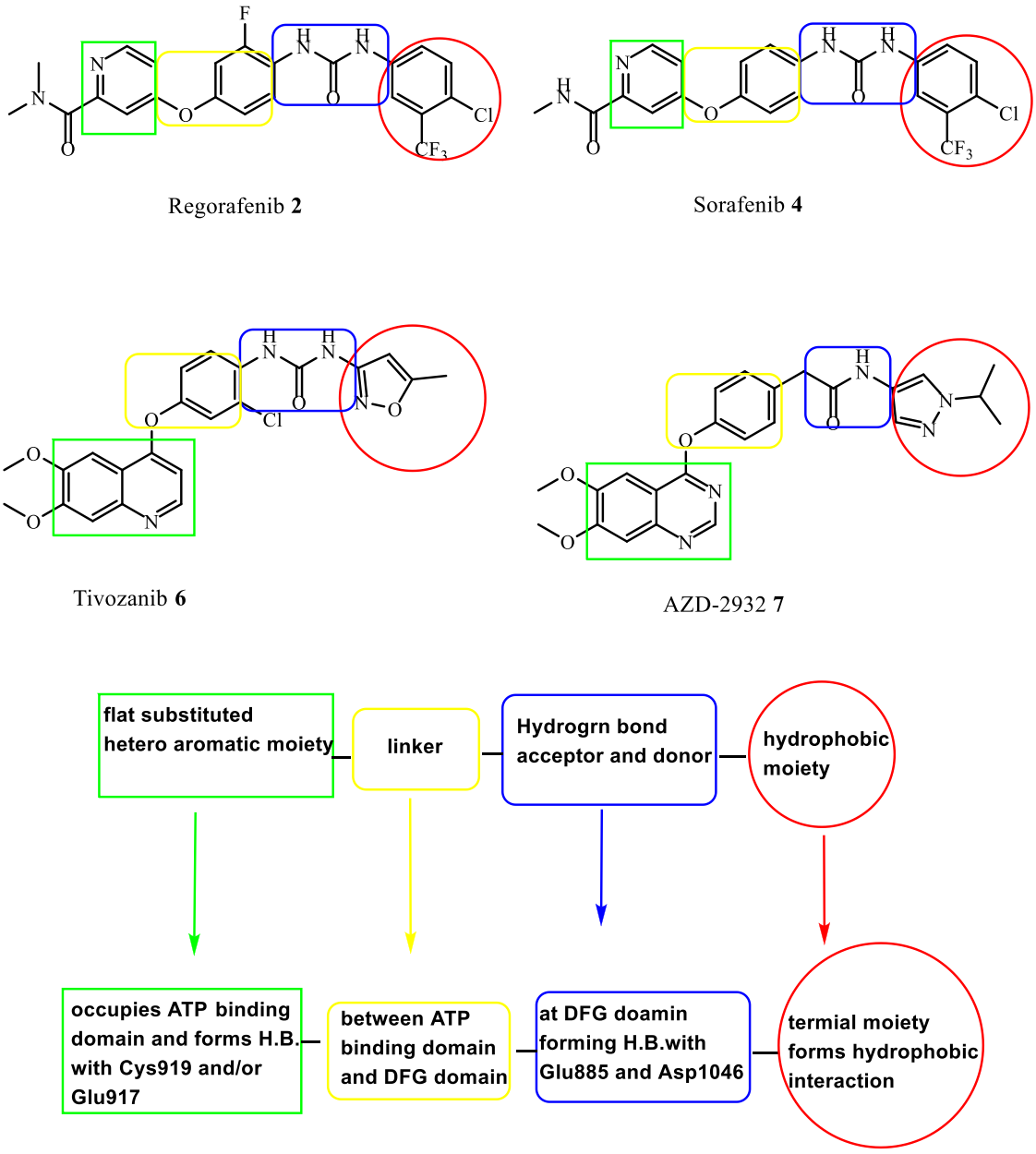

Fig. 2. The common pharmacophoric features of type II VEGFR-2 tyrosine kinase inhibitors.

In the present work we used quinazoline as a scaffold to design compounds consistent with the features of VEGFR-2 inhibitors as shown in Fig. 3. Firstly, we selected substituted quinazoline-2,4-diones as hetero aromatic moiety aiming to occupy ATP binding region and form essential hydrogen bonds with Cys919 and/or Glu917. That is because the quinazoline nucleus represents the hetero aromatic moiety in the potent VEGFR-2 inhibitor AZD-2932 (Fig. 1). We made different substitutions at positions 3 (ethyl & phenyl), 6 (nitro & chloro) and 7 (nitro) of quinazolin-4-one to find the most potent candidate and to establish structure activity relationship. The essential hydrogen bonds can be formed either via nitro group or chloro at positions 6 and 7 or via the nitrogen or oxygen atoms of quinazolin4-one nucleus.

Secondly, we selected amide which served as hydrogen bond acceptor and donor in AZD-2932 (Fig. 1). The amidic group should form essential hydrogen bonds with Glu885 and/or Asp1046 in the DFG domain. In some designed compounds the amide was replaced with oxohydrazide group as an effective hydrogen bond acceptor and donor.

Thirdly, substituted and unsubstituted phenyl rings were designed as terminal hydrophobic groups to form hydrophobic interactions with the allosteric pocket. Palin, 4-methoxy (electron donating) and 4-chloro (electron withdrawing) phenyl were chosen to demonstrate the effect of both substitution and electron density on the phenyl ring on the biological effect.

2. Results and discussion

2.1. Chemistry

The strategy to obtain the target compounds was as follow; firstly, four intermediate compounds (**10$_{a-c}$** and **14**) were prepared as illustrated in Scheme 1. The intermediates **10$_{a-c}$** were prepared by addition of chloroacetyl chloride **9** drop wise to a solution of an appropriate amine, namely aniline, 4-chloroaniline and 4-methoxyaniline [31]. Ethyl benzoate (**12**) was obtained by refluxing benzoic acid with catalytic amount of conc. H_2SO_4 in absolute ethanol [32]. Refluxing compound **12** with hydrazine hydrate in ethanol afforded the corresponding

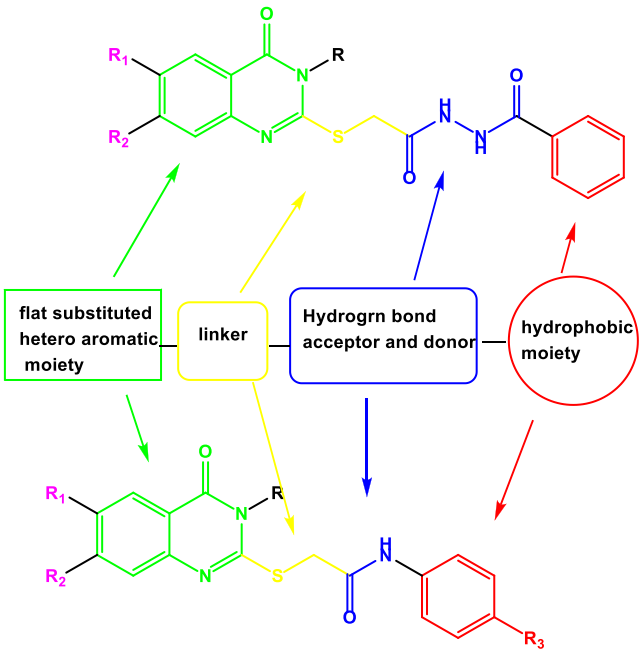

Fig. 3. Model of the designed final compounds as VEGFR-2 kinase inhibitors with the relevant pharmacophoric features.

hydrazide **13** [31].

Treatment of benzohydrazide **13** in DCM with chloro acetylchloride in the presence of triethyl amine as a base under ice cooling gave the intermediate **14** [33].

Secondly, several salts of substituted mercaptoquinazolin-4-one **18$_{a-f}$** were prepared as illustrated in Scheme 2. Refluxing a mixture of substituted anthranilic acid namely 5-chloroanthranilic, 5-nitroanthranilic and 4-nitroanthranilic acid and an appropriate isothiocyanate namely ethyl isothiocyanate and phenyl isothiocyanate in absolute ethanol in the presence of Et_3N afforded the corresponding substituted 2-mercaptoquinazolin-4(3*H*)-one **17$_{a-f}$**. Treatment of compounds **17$_{a-f}$** with equimolar amount of KOH afforded the corresponding salts **18$_{a-f}$**.

Finally, refluxing the potassium salts of quinazolinone **18$_{a-f}$** with an appropriate intermediate compound (**10$_{a-c}$** and **14**) gave the corresponding final compounds **19**–**37** as illustrated in Scheme 2.

IR spectra of the final compounds show that intense bands at about 1535 and 1345 cm^{-1} were recoded specific to compounds containing nitro group. Carbonyls of secondary amide were detected as strong signals from about 1650 to 1701 cm^{-1}. The intense amide II band appeared from 1516 to 1554 cm^{-1}. While carbonyls of quinazolinone nucleus were detected from about 1630 to 1681 cm^{-1}.

^1H NMR spectra of the final compounds show the appearance of singlet signal of two protons integration at about 4.20 ppm which indicates the presence of methylene group flanked between carbonyl group and sulfur atom. With respect to 3-ethylquinazolinone derivatives, two peaks are specific to them, the first is triplet of 3 protons integration and appeared at about 1.33 ppm while the other detected at about 4.14 ppm as quartet of 2 protons integration. Appearance of singlet signal at about 3.72 ppm is characteristic of methoxy containing derivatives. Presence of D_2O exchangeable singlet peak of single proton at about 10.40 ppm is attributed to NH of amide group. While spectra of oxohydrazide containing derivatives revealed two exchangeable singlet peaks at about 10.40 and 10.50 ppm.

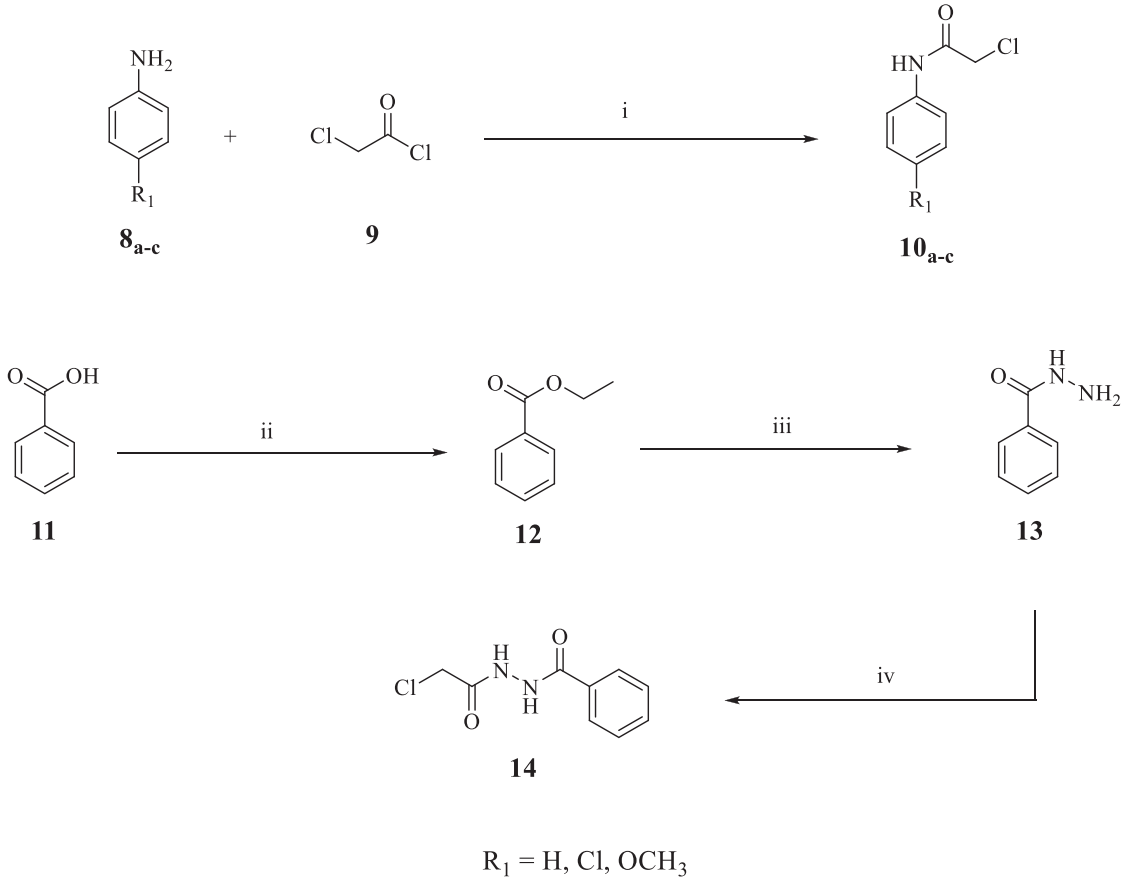

Scheme 1. General procedures for synthesis of intermediates. i: DCM,Et_3N, ice bath. ii: absolute ethanol, conc. H_2SO_4, reflux, 4 h. iii: NH_2NH_2, ethanol, reflux, 8 h. iv: $ClCOCH_2Cl$, DCM, Et_3N, ice bath.

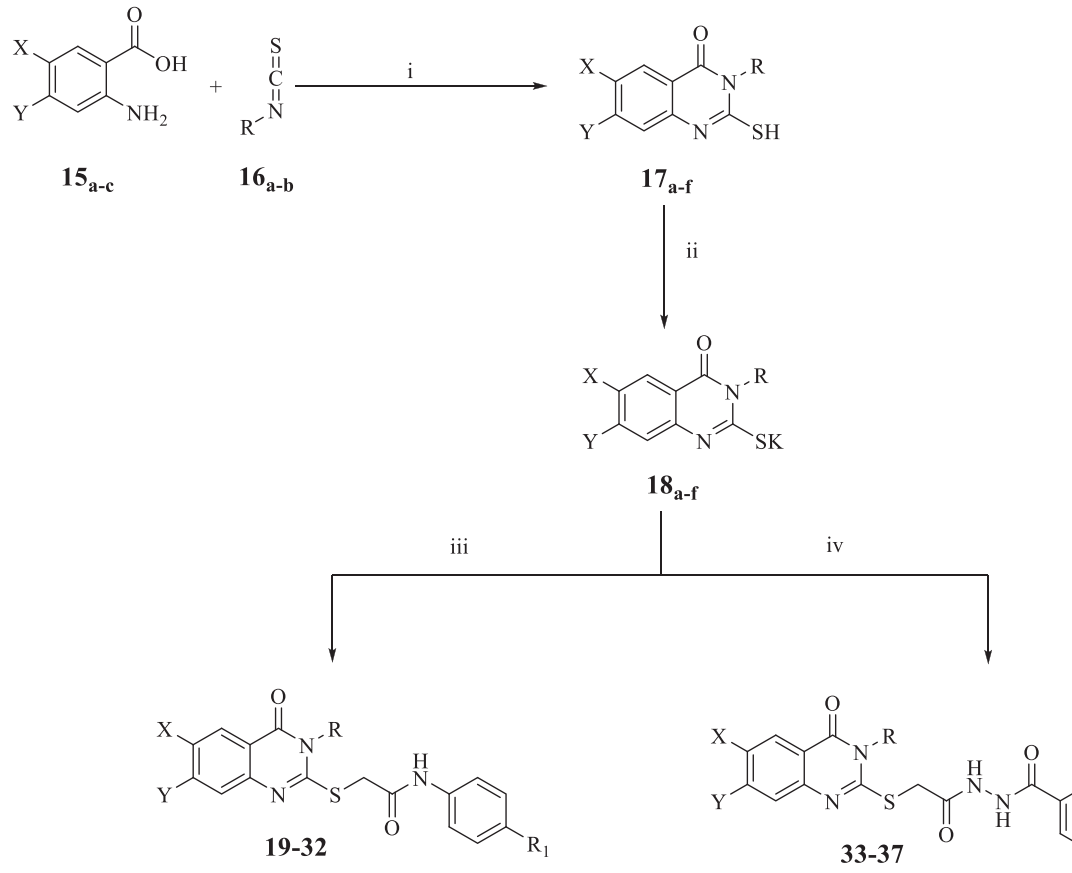

Comp. no.	X	Y	R	R_1
19	H	NO_2	C_2H_5	H
20	H	NO_2	C_2H_5	Cl
21	H	NO_2	C_2H_5	OCH_3
22	H	NO_2	C_6H_5	H
23	H	NO_2	C_6H_5	Cl
24	H	NO_2	C_6H_5	OCH_3
25	Cl	H	C_2H_5	H
26	Cl	H	C_2H_5	Cl
27	Cl	H	C_2H_5	OCH_3
28	Cl	H	C_6H_5	H
29	Cl	H	C_6H_5	Cl
30	Cl	H	C_6H_5	OCH_3
31	NO_2	H	C_2H_5	H
32	NO_2	H	C_6H_5	H

Comp. no.	X	Y	R
33	H	NO_2	C_2H_5
34	Cl	H	C_2H_5
35	Cl	H	C_6H_5
36	NO_2	H	C_2H_5
37	NO_2	H	C_6H_5

Scheme 2. General procedure for synthesis of final compounds. i: absolute ethanol, ET_3N, reflux, 4 h. ii: alc. KOH, heating. iii: compounds 10a-c, KI, acetonitrile, reflux, 2 h. iv: compound 14, KI, acetonitrile, reflux, 2 h.

2.2. Biological testing

2.2.1. In vitro VEGFR-2 tyrosine kinase inhibitory assay

All target compounds were evaluated for their VEGFR-2 tyrosine kinase inhibitory activity. The concentrations that caused 50% enzyme inhibition (IC_{50}) were determined along with IC_{50} of pazopanib as a reference drug.

The results presented in Table 1 indicate that many compounds exhibited potent VEGFR-2 tyrosine kinase inhibition with IC_{50} more or less than that of pazopanib. Compound **36** was found to be the most potent canditate as it demonstrated $IC_{50} = 4.6 \pm 0.06$ μM. it was more potent than pazopanib which showed $IC_{50} = 4.8 \pm 0.07$ μM.

Compounds **37, 28, 35** and **31** were weaker than pazopanib but close to it. They showed $IC_{50} = 4.9 \pm 0.07$, 5.4 ± 0.08, 6.6 ± 0.11 and 6.6 ± 0.13 μM, respectively.

Compounds **34, 25, 29, 32, 27, 30** and **33** should also be considered as they showed potency exceeding half that of pazopanib.

The data indicate the particular significance of oxohydrazide containing 6-nitroquinazolin-4(3*H*)-one derivatives especially compounds **36** and **37**.

Table 1
IC_{50} of *in vitro* VEGFR-2 kinase inhibitory assay for all target compounds and Pazopanib.

Serial	Comp. no.	VEGFR-2 tyrosine kinase IC_{50} (μM)
1	**19**	13.7 ± 0.55
2	**20**	11.3 ± 0.24
3	**21**	10.7 ± 0.21
4	**22**	12.8 ± 0.45
5	**23**	11.1 ± 0.35
6	**24**	10.5 ± 0.22
7	**25**	7.6 ± 0.13
8	**26**	12.3 ± 0.38
9	**27**	9.3 ± 0.20
10	**28**	5.4 ± 0.08
11	**29**	8.5 ± 0.17
12	**30**	9.3 ± 0.19
13	**31**	6.6 ± 0.13
14	**32**	8.5 ± 0.18
15	**33**	9.3 ± 0.14
16	**34**	7.5 ± 0.12
17	**35**	6.6 ± 0.11
18	**36**	4.6 ± 0.06
19	**37**	4.9 ± 0.07
20	Pazopanib	4.8 ± 0.07

2.2.2. *In vitro antiproliferative activity assay*

Nine Compounds of significant VEGFR-2 kinase inhibition were selected for further *in vitro* antitumor investigation along with doxorubicin as a reference drug. The assay was carried out against three human tumor cell lines; hepatocellular carcinoma (HepG2), prostate cancer (PC3), and mammary gland cancer (MCF-7). The concentrations caused 50% inhibition of cancer cell growth (IC_{50}) were presented in Table 2.

The obtained results showed that six compounds are of strong to moderate antiproliferative activity against the tested cell lines. The data also demonstrated that HepG2 cell line is the most sensitive cell line to the effect of the new derivatives, in particular compound **36**.

Compound **36** was found to be the most potent derivative and had demonstrated IC_{50} = 17.23 ± 1.5, 26.10 ± 2.2 and 30.85 ± 2.3 μg/mL against HepG2, PC3 and MCF-7, respectively. Compound **34** was the second most active compound with IC_{50} = 21.68 ± 1.9, 25.49 ± 2.0 and 33.70 ± 2.5 μg/mL against HepG2, PC3 and MCF-7, respectively. Compounds **31, 28, 35** and **37** exhibited moderate activity. Despite of compounds **25, 32** and **29** demonstrated weak anticancer activity, no compound was found to be very weak or inactive.

It is noticeable that compound **36** was the most potent candidate in both VEGFR-2 inhibitory assay and antitumor assay.

Table 2
IC_{50} of *in vitro* antiproliferative and cytotoxicity assay on tumor cell lines, HePG2, PC3 and MCF-7 and on normal cell line WI-38 for the selected nine compounds. [a] IC_{50} values are the mean ± S.D. of three separate experiments.[b] IC_{50} (μg/mL): 1–10 (very strong), 11–25 (strong), 26–50 (moderate), 51–100 (weak).[C] ND: Not determined.

Serial	Comp. no.	IC_{50} (μg/mL)[a,b]			
		HepG2	PC3	MCF-7	WI-38
7	**25**	54.43 ± 3.7	58.01 ± 3.9	62.82 ± 3.8	205.37 ± 1.7
10	**28**	36.27 ± 2.9	45.26 ± 3.0	46.33 ± 3.2	181.09 ± 1.6
11	**29**	71.20 ± 4.1	82.55 ± 4.5	65.18 ± 3.9	167.44 ± 1.4
13	**31**	32.60 ± 2.5	34.09 ± 2.6	42.91 ± 3.1	119.75 ± 1.1
14	**32**	67.20 ± 3.9	89.35 ± 4.7	71.98 ± 4.1	246.12 ± 1.7
16	**34**	21.68 ± 1.9	25.49 ± 2.0	33.70 ± 2.5	105.33 ± 1.1
17	**35**	40.63 ± 3.2	37.16 ± 2.8	35.38 ± 2.6	154.37 ± 1.2
18	**36**	17.23 ± 1.5	26.10 ± 2.2	30.85 ± 2.3	145.93 ± 1.1
19	**37**	44.21 ± 3.5	48.83 ± 3.4	52.49 ± 3.6	161.76 ± 1.3
21	Doxorubicin	7.94 ± 0.6	8.87 ± 0.6	6.75 ± 0.4	ND[c]

2.2.3. *Selective cytotoxicity test*

One very important criterion of good anticancer agent is to be of minimum or no side effect on normal cells. It can be achieved if the agent has high degree of selectivity to cancer cell. So that safety of the target compounds was further evaluated by *in vitro* cytotoxicity assay against the normal human lung fibroblasts cell line (WI-38).

The results presented in Table 2 show that it is typical of all tested compounds to have good degree of selectivity as their effect against normal cell line was far weaker than that against cancer cell lines. In particular, compound **36** which demonstrated selectivity indexes equal 8.47, 5.59 and 4.73 to HepG2, PC3 and MCF-7 cancer cell lines, respectively.

The data presented in Tables 1 & 2 point to Compound **36** as the most significant candidate. So that it was selected to further evaluation by two more biological testing; effect on cell cycle progression and apoptosis induction testing.

2.2.4. *Correlation of cytotoxicity with VEGFR-2 inhibition*

Results of VEGFR-2 inhibitory assay show the ability of our compounds to inhibit VEGFR-2 kinase. To examine to what extent the VEGFR-2 inhibition is the cause of antitumor effects of our compounds, IC_{50} of VEGFR-2 inhibition were plotted against their corresponding antiproliferative ones in simple linear regression setting [34]. The obtained coefficients of determination (R^2) imply the correlation between the VEGFR-2 inhibition and the induced cytotoxicity. The R^2 values for HepG2, PC3, and MCF-7 were 0.4633, 0.4292, and 0.3775, respectively (Fig. 4). Such R^2 values indicate that the VEGFR-2 inhibition accounts to a good extent for the cytotoxicity in the tested cell lines.

2.2.5. *Effect on cell cycle progression.*

Cell cycle analysis was carried out for evaluation the effect of compound **36** on HepG2 growth at different cell cycle phases. The obtained results showed that compound **36** can arrest cell growth cycle at G2/M phase. Fig. 5 illustrates the significant differences in the percent of cells accumulation at G2/M and pre G1 phases between control HepG2 cells and HepG2 cells treated with compound **36**.

2.2.6. *Induction of apoptosis*

Induction of apoptosis in HepG2 cells by compound **36** was also evaluated. The results illustrated in Fig. 6 show that the apoptosis percentage of control HepG2 is significantly increased from 2.37% to 18.33% upon treating with compound **36**. On the other side, necrosis is increased slightly from 1.17% to 2.44%. These data indicate that compound **36** induces cancer cell apoptosis rather than necrosis.

2.3. *In silico studies*

2.3.1. *Docking studies*

To get insights on the binding pattern of target compounds into VEGFR-2 binding site, molecular docking was performed using Molecular Operating Environment (MOE) software. The crystal structure of the enzyme complexed with pyrrolopyrimidine inhibitor was obtained from protein data bank website (PDB code 3VHE). Validation of docking process was carried out by redocking the ligand compound into the active site of the receptor. The ligand was found to demonstrate the same binding mode obtained by X-ray crystal structure with root mean square deviation (RMSD) = 0.42 with free binding energy = -9.34 Kcal/mol.

Fig. 7 and Fig. 8 show that the ligand exhibited four hydrogen bonds; one with Asp1046 and two with Glu885 via its urea moiety; the fourth hydrogen bond was to Glu917 via NH of pyrimidine nucleus. Moreover, it exhibited a further arene-H interaction with Leu840.

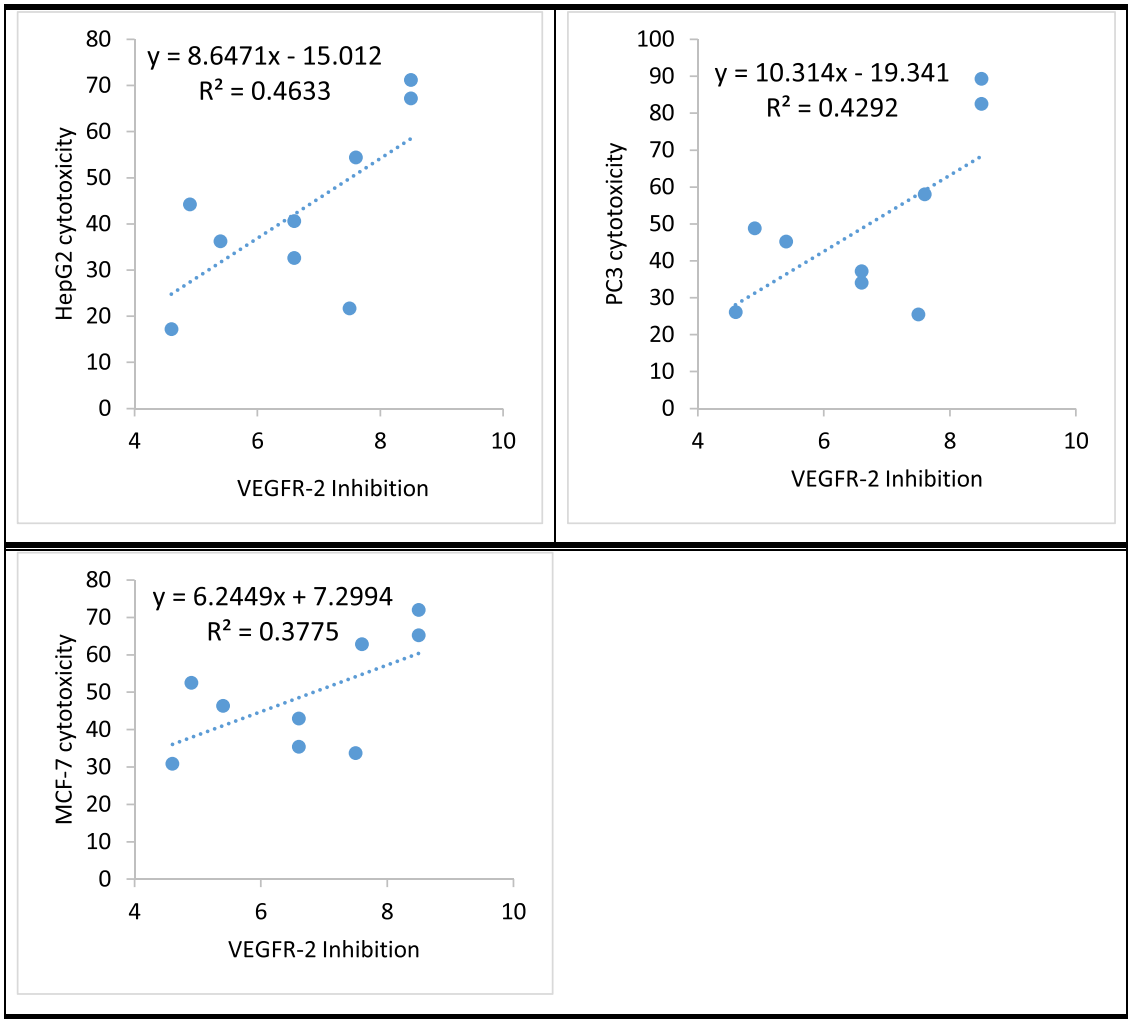

Fig. 4. Correlation of cytotoxicity with VEGFR-2 inhibition on three cell line models HepG2, PC3 and MCF-7.

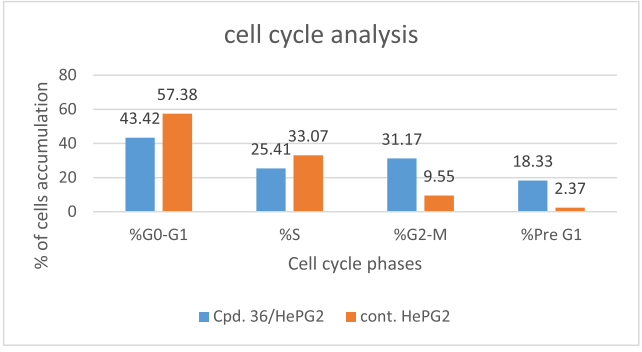

Fig. 5. Effect of compound 36 on percent accumulation of HePG2 cells at different phases of cell cycle compared with untreated HePG2 cells.

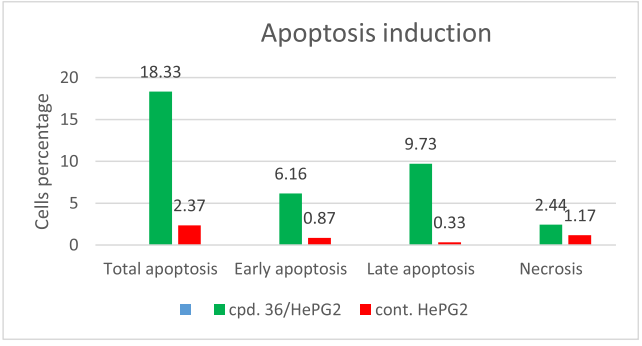

Fig. 6. Effect of compound 36 on HepG2 cells apoptosis and necrosis compared with control HepG2 cells.

According to the binding pattern, our compounds can be divided into two categories; the first showed a binding mode consistent with the design and similar to the binding pattern of the ligand. This category includes compounds **20, 21, 26, 27, 31, 33, 34** and **36**.

Fig. 9 and Fig. 10 show that compound **36** revealed three hydrogen bonds with the three essential amino acids in a correct manner consistent with the design purpose. It made hydrogen bonds with Glu885 and Asp1046 via its oxohydrazide group which was designed to occupy DFG domain. The third hydrogen bond was formed between Cys919 and the nitro group attached to quinazolin-4-one nucleus which was designed to occupy ATP binding domain. Fig. 11 illustrates that the compound **36** and the ligand accommodated the pocket in the same manner which is consistent with the design to a great extent. As the hetero aromatic moiety of both occupied ATP binding domain. At the same time the urea of the ligand and oxohydrazide group of compound **36** occupied the DFG domain.

Fig. 12 and Fig. 13 show the correct binding pattern of compound **33**. As can be seen a hydrogen bond is formed with Glu885 via oxohydrazide

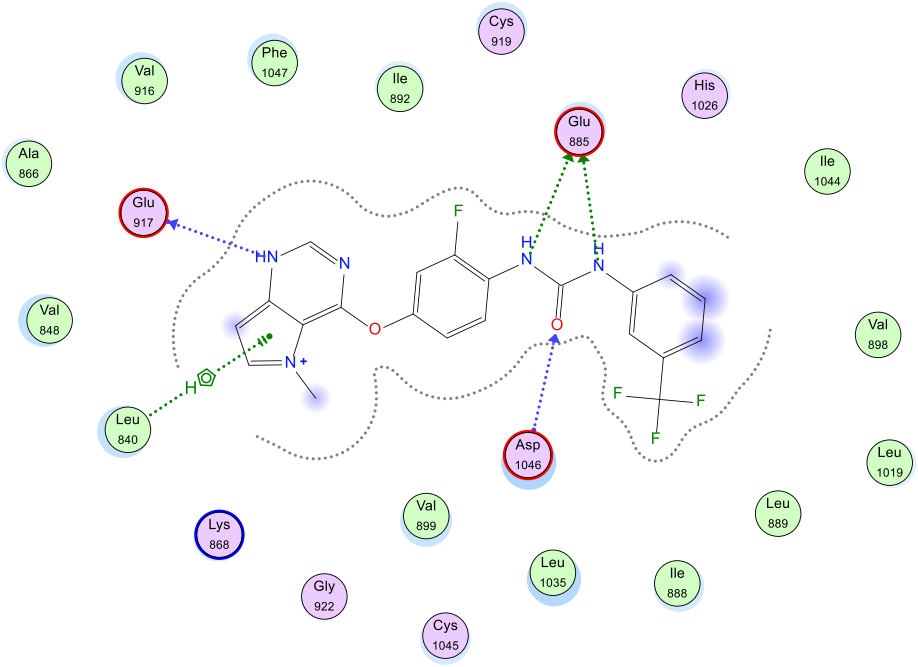

Fig. 7. The binding pattern of the ligand to VEGFR-2 exhibited four essential hydrogen bonds with Glu885, Asp1046 and Glu917 as well as one arene-H interaction with Leu840 (2D image).

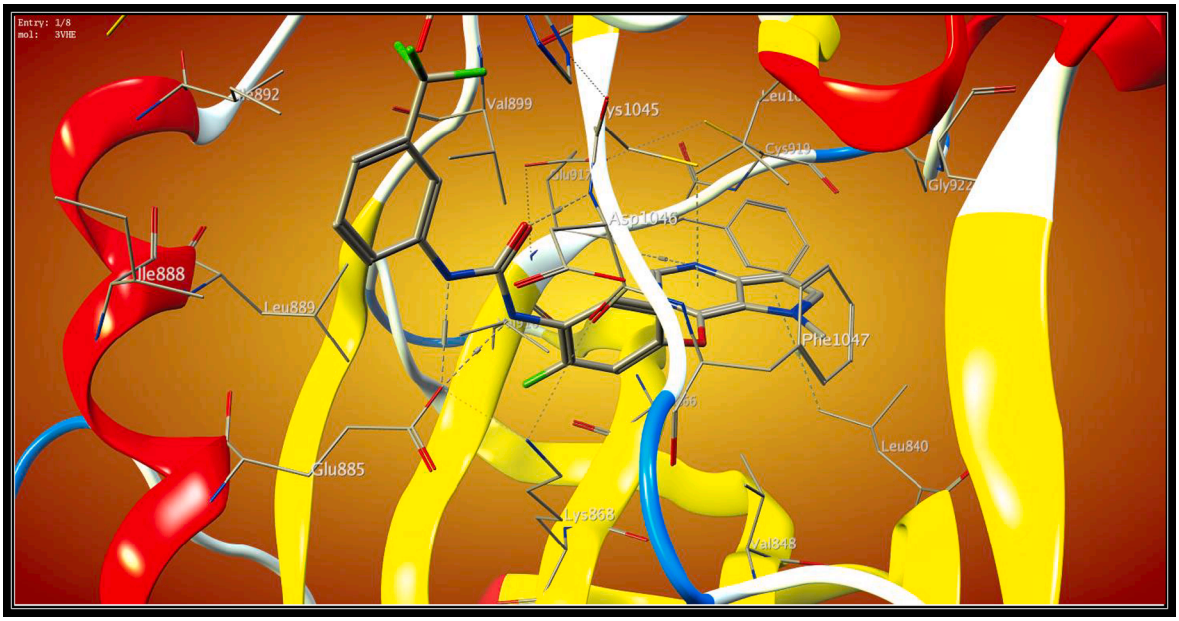

Fig. 8. 3D image for binding of the pyrrolopyrimidine ligand with VEGFR-2, four essential hydrogen bonds were formed with Glu885, Asp1046 and Glu917 as well as one arene-H interaction with Leu840.

moiety and another bond with Cys919 via nitro group attached to the quinazoline nucleus in a manner consistent with the design. Further hydrogen bond can be observed with Lys868. In the same manner Fig. 14 and Fig. 15 reveal the correct binding mode of compound **20** which made two essential hydrogen bonds with Glu885 and Asp1046.

It is noticeable that the ethyl group at position 3 of quinazolin-4-one can accommodate the pocket. So that 3-ethylquinazolin-4-one derivatives showed the correct binding mode. While the phenyl group at position 3 seems to be unable to accommodate the pocket so that all 3-phenylquinazolin-4-one derivatives showed different binding patterns which were not consistent with that of the ligand. Despite of that the binding energies of 3-phenylquinazolin-4-one derivatives were found to be comparable to that of 3-ethylquinazolin-4-one derivatives. That may explain the comparable biological results.

It is noticeable that compound **36** is the single most efficient compound. It is the only one who bound to the three essential amino acids. Furthermore it was of the lowest binding energies (-7.42 Kcal/mol.). These findings clearly explain the superiority of compound **36** in the biological testing.

2.3.2. In silico ADMET analysis

ADMET studies were carried out for final compounds. Pazopanib was

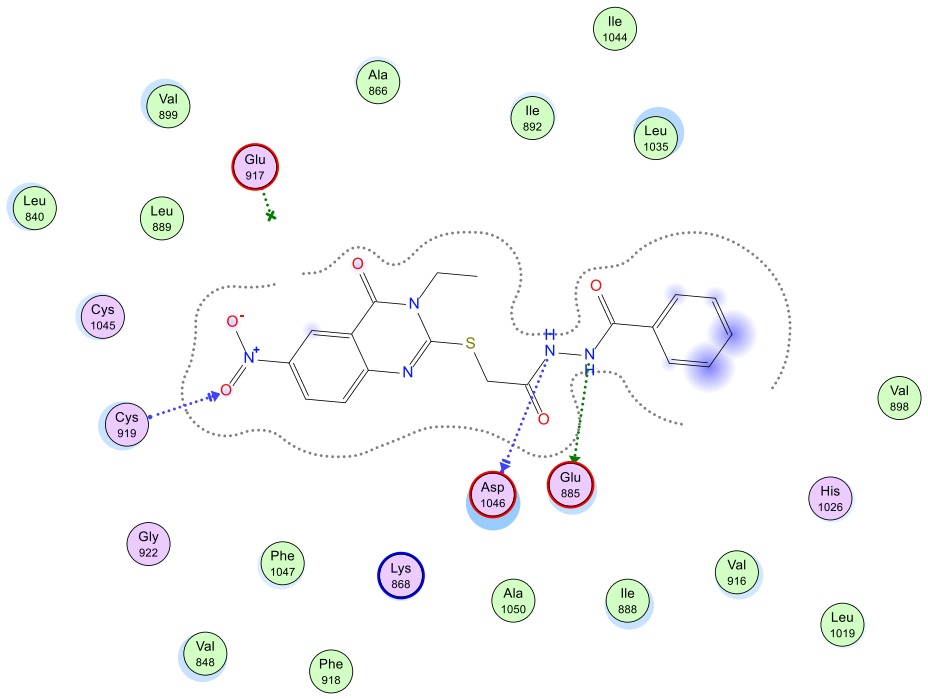

Fig. 9. 2D image shows the binding pattern of compound 36 to VEGFR-2. 3hydrogen bonds can be observed with the essential amino acid residues; Glu885 and Asp1046 via oxohydrazide group; and with Cys919 via nitroquinazolinone moiety.

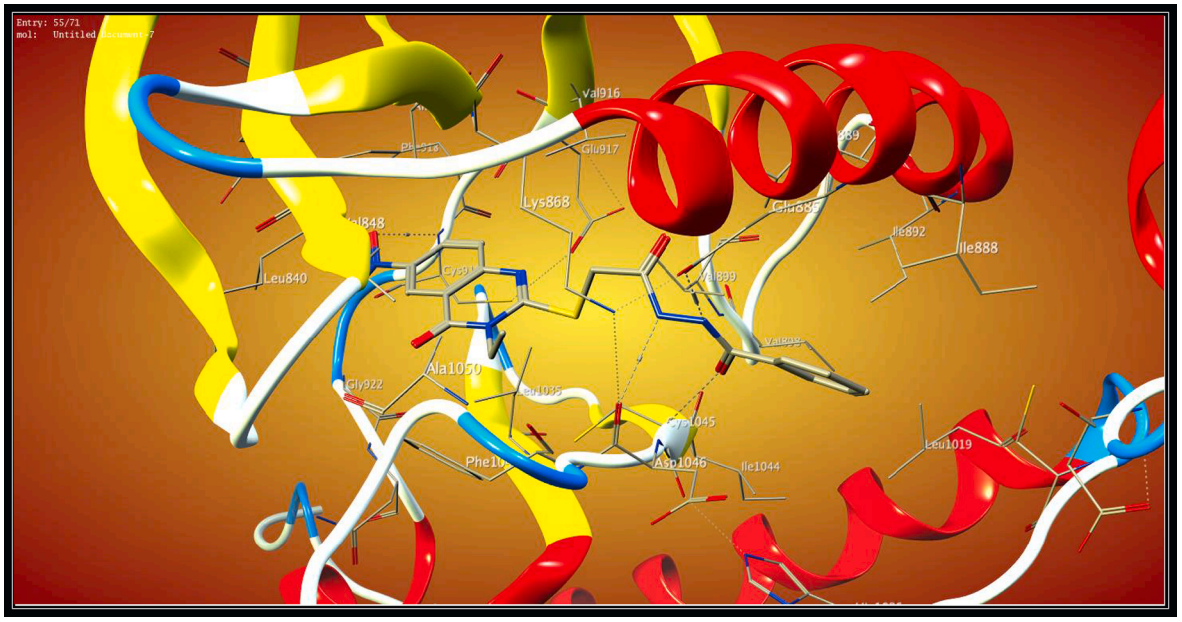

Fig. 10. 3D image for the binding of compound 36 to VEGFR-2 via 3 essential hydrogen bonds with Glu885, Asp1046 and Cys919.

used as reference compound. ADMET studies include many descriptors; i) Blood brain barrier penetration. ii) Intestinal absorption which predicts human intestinal absorption (HIA) after oral administration. iii) Aqueous solubility which predicts the solubility of each compound in water at 25 °C. iv) CYP2D6 binding which predicts cytochrome P450 2D6 enzyme inhibition. v) Plasma protein binding which predicts the fraction of drug bound to plasma proteins in the blood [35]. Discovery studio 4.0 was used to predict ADMET descriptors for all compounds. The predicted descriptors are listed in Table 3.

ADMET - Blood Brain Barrier (BBB) penetration studies predicted that BBB penetration levels of most of synthesized compounds are very low. Accordingly, such compounds were expected to have no CNS side effects. Compounds **25**–**30** were predicted to have high levels of BBB penetration.

Compound **33** and **36** showed good levels of aqueous solubility. On the other hand, the other candidates were expected to have low or very low aqueous solubility.

Intestinal absorption is defined as a percentage absorbed compound from the gut wall [36]. A well-absorbed compound is one that at least 90% absorbed into the bloodstream in humans [37]. According to the ADMET studies, absorption levels of compounds **19**–**21, 25**–**28, 30, 31, 34,** and **35** appeared in the good range, while compounds **22**–**24, 29,**

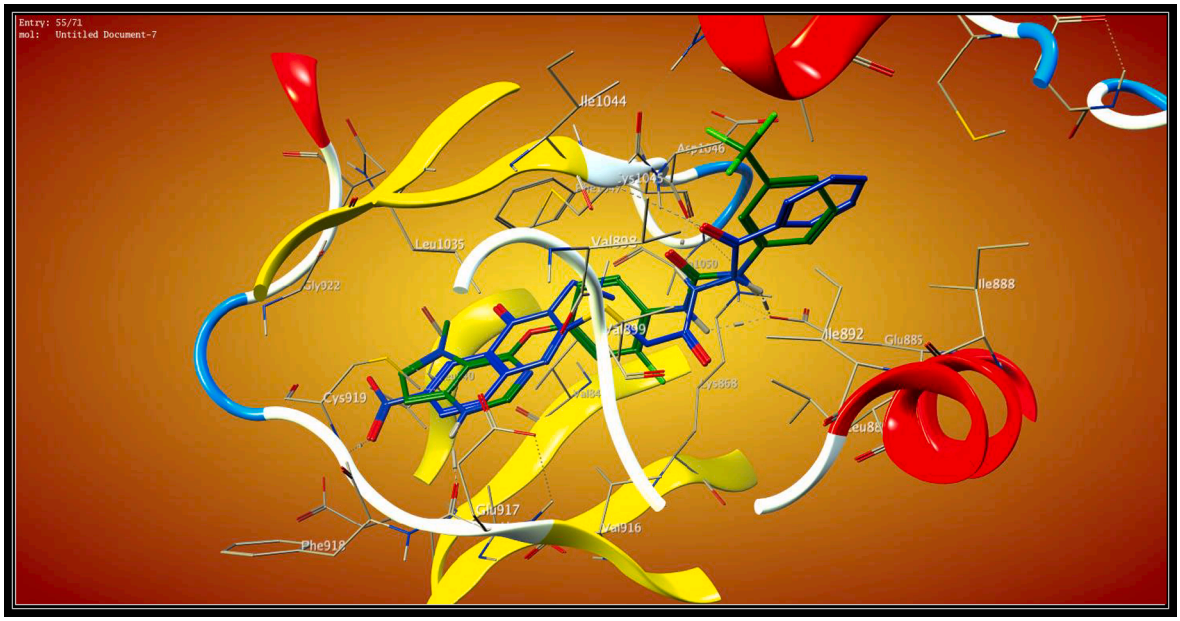

Fig. 11. 3D image shows the overlay of compound 36 (blue colored molecule) and the ligand (green colored one). (For interpretation of the references to colour in this figure legend, the reader is referred to the web version of this article.)

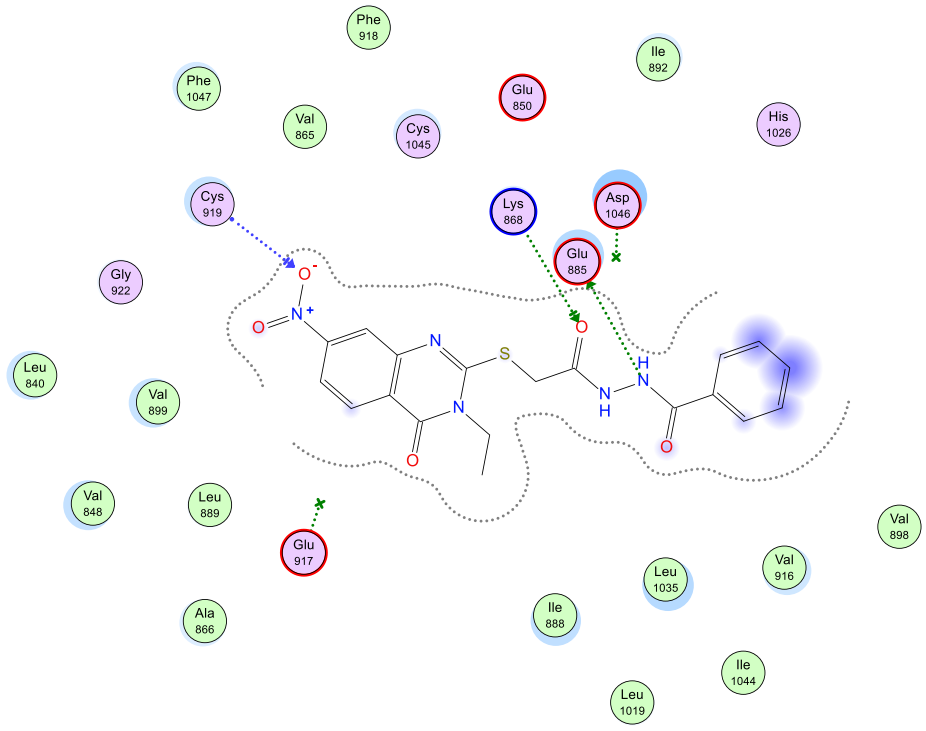

Fig. 12. 2D binding pattern of compound 33, 3 hydrogen bonds were formed with Cys919, Glu885 and Lys868.

32, 33, and **36** showed moderate levels of intestinal absorption. In contrary, compound **37** was predicted to have poor level of intestinal absorption.

The cytochrome P450 2D6 (CYP2D6) model predicts CYP2D6 enzyme inhibition using 2D chemical structure as input. CYP2D6 is involved in the metabolism of a wide range of drugs and hence its inhibition is expected to cause drug drug interactions. Therefore, CYP2D6 inhibition experiment is required as part of the regulatory procedures in the drug discovery and development process [38]. The obtained results predicted that all compounds have the advantage of non-inhibition of CYP2D6. Consequently, liver dysfunction side effect is not expected upon administration of these compounds.

The plasma protein binding model predicts whether a compound is likely to be highly bound (>= 90% bound) to carrier proteins in the blood. All compounds were expected to bind plasma protein over than more than 90% except compounds **21** and **36** (Fig. 16)

2.4. Structure activity relationship (SAR)

On the basis of the obtained results SAR can be established to the

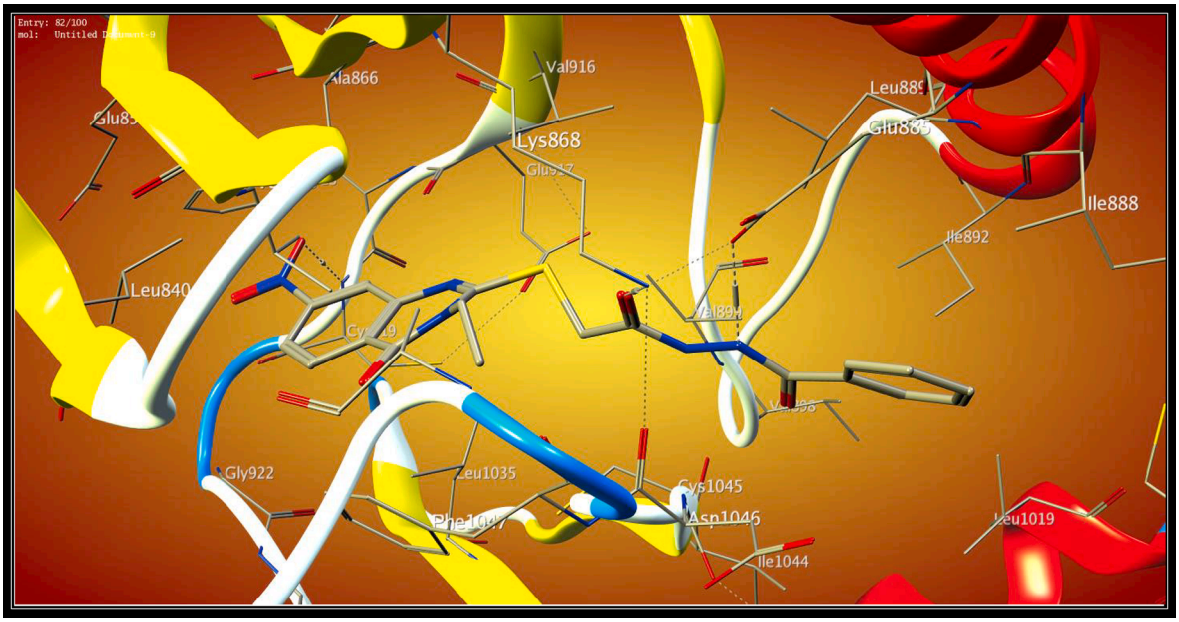

Fig. 13. 3D image for binding pattern of compound 33, 3 hydrogen bonds were formed with Cys919, Glu885 and Lys868.

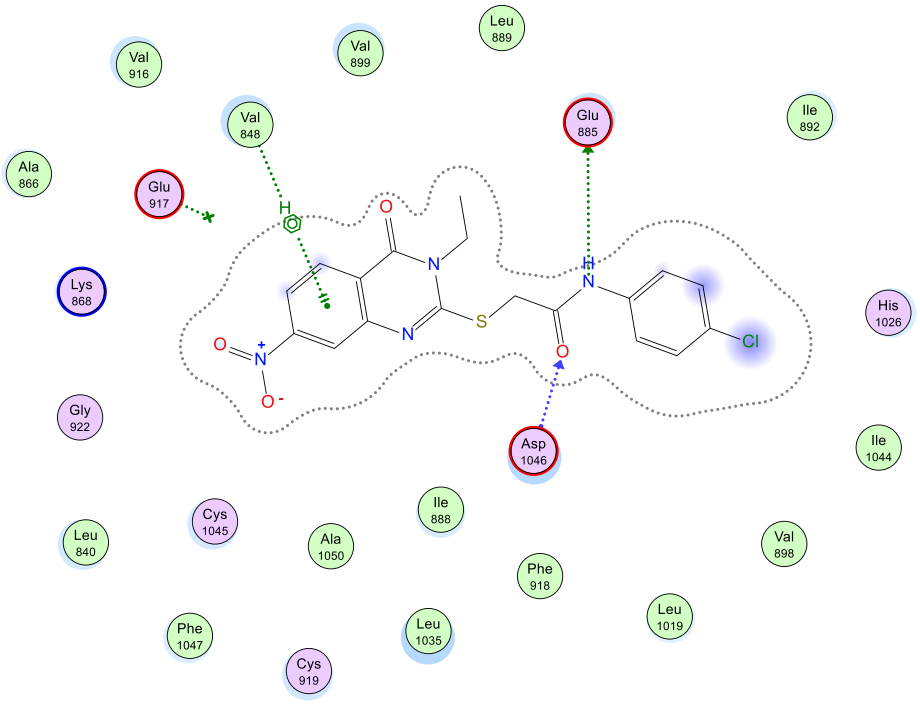

Fig. 14. 2D image for binding pattern of compound 20, it shows hydrogen bonds with the essential amino acid residues Glu 885 and Asp1046 as well as arene-H interaction with Val848.

final compounds as follow

1- Nitro group at position 6 is far better than position 7 of quinazolin-4-one. That may be explained by that the substituent at position 6 is likely to be oriented towards the essential amino acid Cys919. Hence the nitro group at position 6 is able to form hydrogen bond with Cys919. While the substituent at position 7 is oriented away from Cys919.
2- Nitro group at position 6 of quinazolin-4-one is better than chlorine atom.
3- Chlorine atom at position 6 of quinazolin-4-one is more significant than nitro group at position 7. Because it is likely that position 6 is the correct position to orient the substituent to form hydrogen bond with Cys919.
4- Ethyl group at position 3 of quinazolin-4-one is far better than phenyl with regard to design of VEGFR-2 inhibitors type II.
5- *N*-oxohydrazide group is of a significant effect rather than amidic group.
6- It was also found that the terminal plain phenyl has better activity than substituted one.

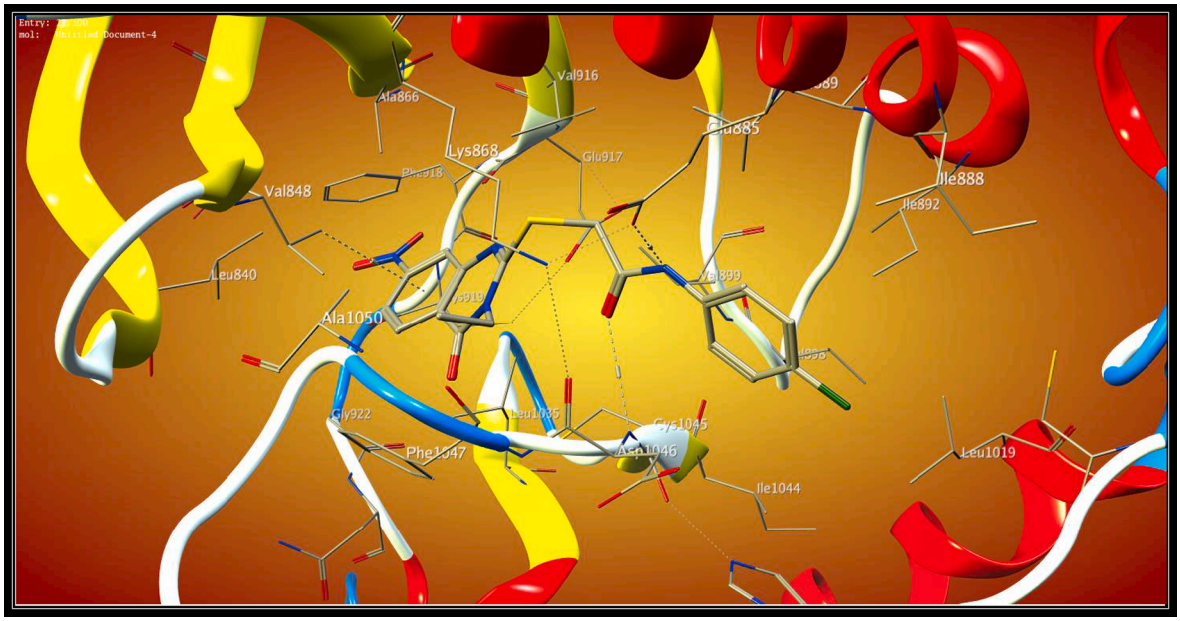

Fig. 15. 3D image for binding pattern of compound 20, it shows hydrogen bonds with the essential amino acid residues Glu 885 and Asp1046 as well as arene-H interaction with Val848.

Table 3
: Predicted ADMET for the designed compounds and reference drugs.

Comp.	BBB level [a]	Solubility level [b]	Absorption level [c]	CYP2D6 prediction [d]	PPB prediction [e]
19	4	2	0	FALSE	TRUE
20	4	2	0	FALSE	TRUE
21	4	2	0	FALSE	FALSE
22	4	2	1	FALSE	TRUE
23	4	1	1	FALSE	TRUE
24	4	2	1	FALSE	TRUE
25	1	2	0	FALSE	TRUE
26	1	2	0	FALSE	TRUE
27	2	2	0	FALSE	TRUE
28	1	1	0	FALSE	TRUE
29	1	1	1	FALSE	TRUE
30	1	1	0	FALSE	TRUE
31	4	2	0	FALSE	TRUE
32	4	2	1	FALSE	TRUE
33	4	3	1	FALSE	TRUE
34	3	2	0	FALSE	TRUE
35	4	2	0	FALSE	TRUE
36	4	3	1	FALSE	FALSE
37	4	2	2	FALSE	TRUE
Pazopanib	4	1	1	FALSE	TRUE

[a] BBB level, blood brain barrier level, 0 = very high, 1 = high, 2 = medium, 3 = low, 4 = very low.
[b] Solubility level, 1 = very low, 2 = low, 3 = good, 4 = optimal.
[c] Absorption level, 0 = good, 1 = moderate, 2 = poor, 3 = very poor.
[d] CYP2D6, cytochrome P2D6, TRUE = inhibitor, FALSE = non inhibitor.
[e] PBB, plasma protein binding, FALSE means less than 90%, TRUE means more than 90%

3. Conclusion

In our effort to develop new effective anticancer agents, new nineteen quinazolinone derivatives were designed, synthesized and biologically evaluated. The design is mainly based on trisubstituted quinazoline-4(3*H*)-one as a scaffold on which the pharmacophoric features of VEGFR-2 kinase inhibitors is built. The data obtained from VEGFR-2 tyrosine kinase inhibitory assay strongly support the significance of VEGFR-2 kinase features illustrated in Fig. 2. At the same time the data suggest that 3-ethyl-6-nitroquinazoline-4-one scaffold is of considerable importance and it should be considered for future development of new potential VEGFR-2 kinase inhibitor agents. The results also point to the relative importance of oxohydrazide moiety to be incorporated in VEGFR-2 kinase inhibitors design. As it serves as hydrogen bond acceptor and donor superior to amide group. Also on the basis of the obtained results, structure activity relationship of the designed compounds was clearly established. At the same time the antiproliferative assay showed that sensitivity of hepatocellular carcinoma to the designed compounds is more than prostate and breast cancer. Moreover, the data of the present study indicate the considerable importance of **36** to serve as a lead compound for further development of potential anticancer agents targeting VEGFR-2 tyrosine kinase.

4. Materials and methods

4.1. Chemistry

All melting points were obtained by open capillary method on a Gallen lamp Melting point apparatus and were uncorrected. Infrared spectra were recorded on Pye Unicam SP 1000 IR spectrophotometer (KBr discs) and were expressed in wave number (cm^{-1}). ^{1}H NMR and ^{13}C NMR spectra were recorded on a BRUKER 400 MHZ-NMR spectrophotometer. TMS was used as internal standard in deuterated DMSO and chemical shifts were measured in δppm. Mass spectra were recorded on Varian MAT 311-A (70 e.v.). Progresses of the reaction was monitored by TLC using TLC sheets precoated with UV fluorescent silica gel Merck 60 F254 plates and were visualized using UV lamp.

4.1.1. 4.1.1. General method of synthesis of compounds (17_{a-f})

General method of synthesis of compounds **(17_{a-f}).** To a solution of anthranilic acid derivative namely, 4-nitroanthranilic acid, 5-chloroanthranilic acid and 5-nitroanthranilic acid (14.58 mmol) and Et_3N (0.30 g, 0.42 mL, 2.92 mmol) in absolute ethanol (30 mL), an appropriate isothiocyanate namely ethyl and phenyl isothiocyanate (16.04 mmol) was added. The reaction mixture was heated under reflux for 5 h. Then upon cooling to r.t., the obtained precipitate was filtered off and recrystallized from ethanol to afford the corresponding substituted 2-mercaptoquinazolin-4(3*H*)-one derivative [39,40].

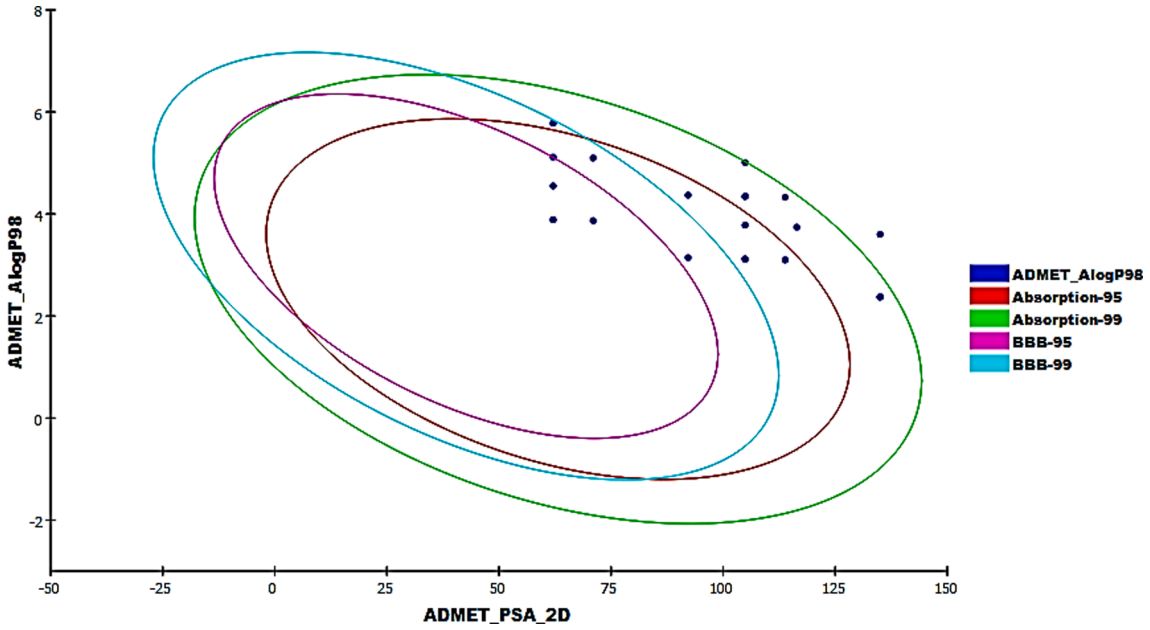

Fig. 16. the expected ADMET profile for final compounds.

4.1.1.1. 4.1.1.1. 6-Chloro-3-ethyl-2-mercaptoquinazolin-4(3H)-one (17$_a$) . 6-Chloro-3-ethyl-2-mercaptoquinazolin-4(3*H*)-one **(17$_a$).** white solid (yield 71.23%); m.p. ˃300 °C; IR (KBr, cm^{-1}): 3197 (NH), 3058 (C—H aromatic), 2986 (C—H aliphatic), 2550 (SH) and 1631 (CO amide); ^{1}H NMR (DMSO-d_6, 400 MHz) δ (ppm): 1.22 (t, *J* = 6.8 *Hz*, 3H, CH_3), 4.41 (q, *J* = 6.8 *Hz*, 2H, CH_2CH_3), 7.35 (d, *J* = 8.4 *Hz*, 1H, Ar-H), 7.74 (dd, *J* = 2.4 & 8.8 *Hz*, 1H, Ar-H), 7.83 (d, *J* = 2.4 *Hz*, 1H, Ar-H), 12.98 (s, 1H, SH).

4.1.1.2. 4.1.1.2. 3-Ethyl-2-mercapto-7-nitro-quinazolin-4(3H)-one (17$_e$) . 3-Ethyl-2-mercapto-7-nitro-quinazolin-4(3*H*)-one **(17$_e$).** White solid (yield 60.05%); m.p. 262–264 °C; IR (KBr, cm^{-1}): 3116 (NH), 3095 (C—H aromatic), 2940, 2890 (C—H aliphatic), 2600 (SH), 1627 (CO amide) and 1534, 1338 (NO_2); ^{1}H NMR (DMSO-d_6, 400 MHz) δ (ppm): 1.24 (t, *J* = 7.2 *Hz*, 3H, CH_3), 4.42 (q, *J* = 6.8 *Hz*, 2H, CH_2CH_3), 8.01 (dd, *J* = 2.0 & 8.8 *Hz*, 1H, Ar-H), 8.11 (d, *J* = 2.0 *Hz*, 1H, Ar-H), 8.14 (d, *J* = 8.8 *Hz*, 1H, Ar-H), 13.16 (s, 1H, SH).

4.1.1.3. 4.1.1.3. 2-Mercapto-7-nitro-3-phenyl-quinazolin-4(3H)-one (17$_f$) . 2-Mercapto-7-nitro-3-phenyl-quinazolin-4(3*H*)-one **(17$_f$).** Yellow solid (yield 54.99%); m.p. 240–242 °C; IR (KBr, cm^{-1}): 3269 (NH), 3090 (C—H aromatic), 2600 (SH), 1658 (CO amide) and 1531, 1353 (NO_2); ^{1}H NMR (DMSO-d_6, 400 MHz) δ (ppm): 7.30 (d, *J* = 6.8 *Hz*, 2H, Ar-H), 7.43 (t, *J* = 7.2 *Hz*, 1H, Ar-H), 7.50 (t, *J* = 7.2 *Hz*, 2H, Ar-H), 8.05 (dd, *J* = 2.0 & 8.8 *Hz*, 1H, Ar-H), 8.17 (d, *J* = 8.8 *Hz*, 1H, Ar-H), 8.21 (d, *J* = 2.0 *Hz*, 1H, Ar-H), 13.30 (s, 1H, SH).

4.1.2. 4.1.2. General procedure of synthesis of compounds (18$_{a-f}$)

General procedure of synthesis of compounds **(18$_{a-f}$)** 2-Mercapto-quinazolin-4(3*H*)-one derivative **(17$_{a-f}$)** was added to alcoholic solution of equimolar amount of potassium hydroxide. The reaction mixture was heated with stirring until a sticky mass was obtained. Upon cooling to r. t. and drying, the corresponding potassium salt was obtained in a quantitative yield. All had melting points above 300 °C.

4.1.3. General procedure of synthesis of final compounds (19–37)

General procedure of synthesis of final compounds **(19–37).** A mixture of an appropriate potassium salt of 2-mercaptoquinazolin-4 (3*H*)-one **18$_{a-f}$** (0.65 mmol) and an intermediate compound (**3$_{a-c}$** and **7$_{a, b}$**) (0.65 mmol) was heated under reflux for 2 h in acetonitrile (20 mL) in the presence of a catalytic amount of KI. The reaction mixture was then left to cool and diluted with cold water (50 mL) to give a precipitate. The obtained precipitate was collected by filtration, washed with water, dried and then crystallized from ethanol to afford the corresponding final compound.

4.1.3.1. 2-[(3-Ethyl-7-nitro-4-oxo-3,4-dihydroquinazoline-2-yl)thio]-N-phenylacetamide. (19). 2-[(3-Ethyl-7-nitro-4-oxo-3,4-dihydroquinazoline-2-yl)thio]-*N*-phenylacetamide. **(19).** yellow solid (yield 88.80%). m.p. 190 °C; IR (KBr, cm^{-1}): 3286 (NH), 3082 (C—H aromatic), 2993 & 2943 (C—H aliphatic), 1693 (CO amide), 1651 (CO amide), 1550 (amide II band) and 1535, 1342 (NO_2); ^{1}H NMR (DMSO-d_6, 400 MHz) δ (ppm): 1.33 (t, *J* = 7.0 *Hz*, 3H, CH_3CH_2), 4.14 (q, *J* = 7.0 *Hz*, 2H, CH_3CH_2), 4.27 (s, 2H, CH_2CO), 7.06 (t, *J* = 7.4 *Hz*, 1H, Ar-H phenyl), 7.32 (dd, *J* = 7.4 & 8.0 *Hz*, 2H, Ar-H phenyl), 7.62 (d, *J* = 8.0 *Hz*, 2H, Ar-H phenyl), 8.13 (dd, *J* = 2.2 & 8.7 *Hz*, 1H, Ar-H quinazoline), 8.24 (d, *J* = 2.2 *Hz*, 1H, Ar-H quinazoline), 8.27 (d, *J* = 8.7 *Hz*, 1H, Ar-H quinazoline), 10.45 (s, 1H, D_2O exchangeable, NH). ^{13}C NMR (DMSO-d_6, 400 MHz) δ (ppm): 13.15, 37.36, 40.45, 119.69, 119.79, 121.20, 123.51, 124.01, 129.21, 129.28, 139.36, 147.31, 151.57, 159.46, 159.77, 166.10.

4.1.3.2. N-(4-Chlorophenyl)-2-[(3-ethyl-7-nitro-4-oxo-3,4-dihydroquinazoline-2-yl)thio]-acetamide. (20). *N*-(4-Chlorophenyl)-2-[(3-ethyl-7-nitro-4-oxo-3,4-dihydroquinazoline-2-yl)thio]-acetamide. **(20).** yellow solid (yield 92.20%). m.p. 215 °C; IR (KBr, cm^{-1}): 3344 (NH), 3089 (C—H aromatic), 2974 & 2916 (C—H aliphatic), 1693 (CO amide) and 1539, 1346 (NO_2); ^{1}H NMR (DMSO-d_6, 400 MHz) δ (ppm): 1.33 (t, *J* = 7.0 *Hz*, 3H, CH_3CH_2), 4.14 (q, *J* = 7.0 *Hz*, 2H, CH_3CH_2), 4.27 (s, 2H, CH_2CO), 7.37 (d, *J* = 8.8 *Hz*, 2H, Ar-H phenyl), 7.65 (d, *J* = 8.8 *Hz*, 2H, Ar-H phenyl), 8.13 (dd, *J* = 2.2 & 8.8 *Hz*, 1H, Ar-H quinazoline), 8.21 (d, *J* = 2.2 *Hz*, 1H, Ar-H quinazoline), 8.27 (d, *J* = 8.7 *Hz*, 1H, Ar-H quinazoline), 10.59 (s, 1H, D_2O exchangeable, NH). ^{13}C NMR (DMSO-d_6, 400 MHz) δ (ppm): 13.15, 29.45, 37.30, 119.68, 121.18, 123.54, 127.58, 129.21, 129.24, 130.05, 138.33, 147.30, 151.61, 159.41, 159.79, 166.35. Mass (*m/z*): 420 (M^++2), 418 (M^+), 380, 355 (100%, base peak), 290, 247, 240, 231, 222, 148, 119, 76, 64 and 53.

4.1.3.3. 2-[(3-Ethyl-7-nitro-4-oxo-3,4-dihydroquinazoline-2-yl)thio]-N-(4-methoxyphenyl)acetamide. (21). 2-[(3-Ethyl-7-nitro-4-oxo-3,4-dihydroquinazoline-2-yl)thio]-*N*-(4-methoxyphenyl)acetamide. **(21).** yellow

solid (yield 87.50%). m.p. 185 °C; IR (KBr, cm^{-1}): 3271 (NH), 3097 & 3059 (C—H aromatic), 2993 & 2943 (C—H aliphatic), 1685 (CO amide), 1651 (CO amide), 1550 (amide II band) and 1531, 1342 (NO_2); ^{1}H NMR (DMSO-d_6, 400 MHz) δ (ppm): 1.33 (t, *J* = 7.08 *Hz*, 3H, CH_3CH_2), 3.72 (s, 3H, OCH_3), 4.14 (q, *J* = 7.08 *Hz*, 2H, CH_3CH_2), 4.24 (s, 2H, CH_2CO), 6.88 (d, *J* = 8.96 *Hz*, 2H, Ar-H phenyl), 7.52 (d, *J* = 8.96 *Hz*, 2H, Ar-H phenyl), 8.14 (dd, *J* = 2.28 & 8.72 *Hz*, 1H, Ar-H quinazoline), 8.27 (d, *J* = 2.20 *Hz*, 1H, Ar-H quinazoline), 8.28 (d, *J* = 8.84 *Hz*, 1H, Ar-H quinazoline), 10.30 (s, 1H, D_2O exchangeable, NH). ^{13}C NMR (DMSO-d_6, 400 MHz) δ (ppm): 12.14, 13.16, 41.83, 55.64, 111.41, 114.41, 118.52, 119.86, 121.30, 129.26, 130.07, 139.85, 147.37, 151.65, 155.88, 159.84, 165.60.

4.1.3.4. 2-[(7-Nitro-4-oxo-3-phenyl-3,4-dihydroquinazoline-2-yl)thio]-N-phenylacetamide. ***(22)***. 2-[(7-Nitro-4-oxo-3-phenyl-3,4-dihydroquinazoline-2-yl)thio]-*N*-phenylacetamide. **(22).** yellow solid (yield 85.50%). m.p. 213 °C; IR (KBr, cm^{-1}): 3290 (NH), 3082 & 3043 (C—H aromatic), 2993 (C—H aliphatic), 1693 (CO amide), 1651 (CO amide), 1554 (amide II band) and 1535, 1342 (NO_2); ^{1}H NMR (DMSO-d_6, 400 MHz) δ (ppm): 4.13 (s, 2H, CH_2CO), 7.06 (t, *J* = 7.4 *Hz*, 1H, Ar-H phenyl), 7.32 (dd, *J* = 7.64 & 8.12 *Hz*, 2H, Ar-H phenyl), 7.54 (m, 2H, Ar-H phenyl), 7.62 (m, 5H, Ar-H phenyl), 8.17 (dd, *J* = 2.24 & 8.72 *Hz*, 1H, Ar-H quinazoline), 8.29 (d, *J* = 8.68 *Hz*, 1H, Ar-H quinazoline), 8.34 (d, *J* = 2.04 *Hz*, 1H, Ar-H quinazoline), 10.39 (s, 1H, D_2O exchangeable, NH). ^{13}C NMR (DMSO-d_6, 400 MHz) δ (ppm): 37.87, 119.66, 119.95, 121.30, 124.03, 124.56, 129.29, 129.41, 129.66, 130.18, 130.79, 135.82, 139.33, 147.85, 151.78, 160.22, 160.58, 166.18.

4.1.3.5. N-(4-Chlorophenyl)-2-[(7-nitro-4-oxo-3-phenyl-3,4-dihydroquinazoline-2-yl)thio]acetamide. ***(23)***. *N*-(4-Chlorophenyl)-2-[(7-nitro-4-oxo-3-phenyl-3,4-dihydroquinazoline-2-yl)thio]acetamide. **(23).** yellow solid (yield 80.42%). m.p. 245 °C; IR (KBr, cm^{-1}): 3294 (NH), 3059 & 3039 (C—H aromatic), 2981 & 2920 (C—H aliphatic), 1697 (CO amide), 1658 (CO amide), 1554 (amide II band) and 1527, 1346 (NO_2); ^{1}H NMR (DMSO-d_6, 400 MHz) δ (ppm): 4.12 (s, 2H, CH_2CO), 7.37 (d, *J* = 8.8 *Hz*, 2H, Ar-H phenyl), 7.53 (m, 2H, Ar-H phenyl), 7.62 (m, 5H, Ar-H phenyl), 8.17 (dd, *J* = 2.16 & 8.72 *Hz*, 1H, Ar-H quinazoline), 8.28 (d, *J* = 8.72 *Hz*, 1H, Ar-H quinazoline), 8.31 (d, *J* = 2.04 *Hz*, 1H, Ar-H quinazoline), 10.53 (s, 1H, D_2O exchangeable, NH). ^{13}C NMR (DMSO-d_6, 400 MHz) δ (ppm): 37.82, 119.97, 121.17, 121.26, 124.56, 127.57, 129.21, 129.42, 129.65, 130.18, 130.80, 135.81, 138.30, 147.82, 151.78, 160.21, 160.52, 166.41. Mass (*m/z*): 468 (M^++2), 466 (M^+), 451, 439, 424, 415, 339, 283 (100%, base peak), 261, 250, 231, 223, 88, 84 and 80.

4.1.3.6. N-(4-Methoxyphenyl)-2-[(7-nitro-4-oxo-3-phenyl-3,4-dihydroquinazoline-2-yl)thio]acetamide. ***(24)***. *N*-(4-Methoxyphenyl)-2-[(7-nitro-4-oxo-3-phenyl-3,4-dihydroquinazoline-2-yl)thio]acetamide. **(24).** yellow solid (yield 83.57%). m.p. 210 °C; IR (KBr, cm^{-1}): 3325 & 3209 (NH), 3059 & 3032 (C—H aromatic), 1650 (CO amide), 1631 (CO amide), 1554 (amide II band) and 1530, 1323 (NO_2); ^{1}H NMR (DMSO-d_6, 400 MHz) δ (ppm): 3.72 (s, 3H, OCH_3), 4.10 (s, 2H, CH_2CO), 6.87 (d, *J* = 9.00 *Hz*, 2H, Ar-H phenyl), 7.53 (m, 4H, Ar-H phenyl), 7.62 (m, 3H, Ar-H phenyl), 8.18 (dd, *J* = 2.24 & 8.72 *Hz*, 1H, Ar-H quinazoline), 8.29 (d, *J* = 8.68 *Hz*, 1H, Ar-H quinazoline), 8.35 (d, *J* = 2.12 *Hz*, 1H, Ar-H quinazoline), 10.24 (s, 1H, D_2O exchangeable, NH). ^{13}C NMR (DMSO-d_6, 400 MHz) δ (ppm): 37.79, 55.63, 114.39, 119.94, 121.25, 121.32, 124.57, 129.41, 129.67, 130.17, 130.78, 132.47, 135.83, 147.88, 151.80, 155.87, 160.24, 160.60, 165.62.

4.1.3.7. 2-[(6-Chloro-3-ethyl-4-oxo-3,4-dihydroquinazolin-2-yl)thio]-N-phenylacetamide. ***(25)***. 2-[(6-Chloro-3-ethyl-4-oxo-3,4-dihydroquinazolin-2-yl)thio]-*N*-phenylacetamide. **(25)**. white solid (yield 91.15%). m.p. 180 °C; IR (KBr, cm^{-1}): 3340 (NH), 3066 & 3035 (C—H aromatic), 2997 & 2947 (C—H aliphatic), 1681 (CO amide), 1662 (CO amide) and1550 (amide II band); ^{1}H NMR (DMSO-d_6, 400 MHz) δ (ppm): 1.32 (t, *J* = 7.04 *Hz*, 3H, CH_3CH_2), 4.12 (q, *J* = 7.0 *Hz*, 2H, CH_3CH_2), 4.23 (s, 2H, CH_2CO), 7.06 (t, *J* = 7.36 *Hz*, 1H, Ar-H phenyl), 7.32 (dd, *J* = 7.68 & 8.0 *Hz*, 2H, Ar-H phenyl), 7.47 (d, *J* = 8.72 *Hz*, 1H, Ar-H quinazoline), 7.59 (d, *J* = 7.88 *Hz*, 2H, Ar-H phenyl), 7.79 (dd, *J* = 2.48 & 8.72 *Hz*, 1H, Ar-H quinazoline), 7.99 (d, *J* = 2.36 *Hz*, 1H, Ar-H quinazoline), 10.40 (s, 1H, D_2O exchangeable, NH). ^{13}C NMR (DMSO-d_6, 400 MHz) δ (ppm): 13.31, 37.19, 40.23, 119.68, 120.45, 123.98, 125.76, 128.41, 129.28, 130.42, 135.23, 139.37, 145.86, 157.22, 159.78, 166.10.

4.1.3.8. 2-[(6-Chloro-3-ethyl-4-oxo-3,4-dihydroquinazolin-2-yl)thio]-N-(4-chlorophenyl)acetamide. ***(26)***. 2-[(6-Chloro-3-ethyl-4-oxo-3,4-dihydroquinazolin-2-yl)thio]-*N*-(4-chlorophenyl)acetamide. **(26)**. white solid (yield 91.45%). m.p. 205 °C; IR (KBr, cm^{-1}): 3278 (NH), 3074 & 3043 (C—H aromatic), 2981 & 2920 (C—H aliphatic), 1689 (CO amide), 1658 (CO amide) and 1546 (amide II band); ^{1}H NMR (DMSO-d_6, 400 MHz) δ (ppm): 1.31 (t, *J* = 7.0 *Hz*, 3H, CH_3CH_2), 4.12 (q, *J* = 7.0 *Hz*, 2H, CH_3CH_2), 4.22 (s, 2H, CH_2CO), 7.36 (d, *J* = 8.84 *Hz*, 2H, Ar-H phenyl), 7.44 (d, *J* = 8.72 *Hz*, 1H, Ar-H quinazoline), 7.63 (d, *J* = 8.84 *Hz*, 2H, Ar-H phenyl), 7.79 (dd, *J* = 2.48 & 8.72 *Hz*, 1H, Ar-H quinazoline), 7.99 (d, *J* = 2.44 *Hz*, 1H, Ar-H quinazoline), 10.55 (s, 1H, D_2O exchangeable, NH). ^{13}C NMR (DMSO-d_6, 400 MHz) δ (ppm): 13.32, 37.18, 40.24, 120.49, 121.19, 125.80, 127.51, 128.39, 129.21, 130.44, 135.28, 138.36, 145.86, 157.20, 159.77, 166.31. Mass (*m/z*): 411 (M^++4), 409 (M^++2), 407 (M^+), 379, 345, 336, 332 (100%, base peak), 331, 316, 184, 269, 234, 211, 193, 181, 177, 162, 120, 107, 95, 73 and 47.

4.1.3.9. 2-[(6-Chloro-3-ethyl-4-oxo-3,4-dihydroquinazoline-2-yl)thio]-N-(4-methoxyphenyl)acetamide. ***(27)***. 2-[(6-Chloro-3-ethyl-4-oxo-3,4-dihydroquinazoline-2-yl)thio]-*N*-(4-methoxyphenyl)acetamide. **(27).** white solid (yield 88.32%). m.p. 177 °C; IR (KBr, cm^{-1}): 3248 (NH), 3055 (C—H aromatic), 2989 & 2935 (C—H aliphatic), 1689 (CO amide), 1651 (CO amide) and 1554 (amide II band); ^{1}H NMR (DMSO-d_6, 400 MHz) δ (ppm): 1.31 (t, *J* = 7.12 *Hz*, 3H, CH_3CH_2), 3.72 (s, 3H, OCH_3), 4.12 (q, *J* = 7.08 *Hz*, 2H, CH_3CH_2), 4.20 (s, 2H, CH_2CO), 6.90 (d, *J* = 8.96 *Hz*, 2H, Ar-H phenyl), 7.50 (m, 3H, Ar-H), 7.80 (dd, *J* = 2.48 & 8.72 *Hz*, 1H, Ar-H quinazoline), 8.00 (d, *J* = 2.44 *Hz*, 1H, Ar-H quinazoline), 10.25 (s, 1H, D_2O exchangeable, NH). ^{13}C NMR (DMSO-d_6, 400 MHz) δ (ppm): 13.31, 37.08, 40.22, 55.62, 114.38, 120.45, 121.30, 125.77, 128.44, 130.41, 132.49, 135.25, 145.88, 155.86, 157.25, 159.80, 165.58.

4.1.3.10. 2-[(6-chloro-4-oxo-3-phenyl-3,4-dihydroquinazoline-2-yl)thio]-N-phenylacetamide. ***(28)***. 2-[(6-chloro-4-oxo-3-phenyl-3,4-dihydroquinazoline-2-yl)thio]-*N*-phenylacetamide. **(28).** white solid (yield 90.20%). m.p. 206 °C; IR (KBr, cm^{-1}): 3290 (NH), 3059 & 3039 (C—H aromatic), 1701 (CO amide), 1651 (CO amide) and 1543 (amide II band); ^{1}H NMR (DMSO-d_6, 400 MHz) δ (ppm): 4.09 (s, 2H, CH_2CO), 7.04 (t, *J* = 7.40 *Hz*, 1H, Ar-H phenyl), 7.31 (t, *J* = 7.90 *Hz*, 2H, Ar-H phenyl), 7.51 (m, 2H, Ar-H phenyl), 7.58, (m, 2H, Ar-H phenyl), 7.60 (m, 3H, Ar-H phenyl), 7.62 (d, *J* = 8.70 *Hz*, 1H, Ar-H quinazoline), 7.86, (dd, *J* = 8.70 & 2.50 *Hz*, 1H, Ar-H quinazoline), 8.01 (d, *J* = 2.40 *Hz*, 1H, Ar-H quinazoline), 10.34 (s, 1H, D_2O exchangeable, NH). ^{13}C NMR (DMSO-d_6, 400 MHz) δ (ppm): 37.81, 119.61, 121.37, 123.94, 126.00, 128.59, 129.27, 129.79, 130.09, 130.49, 130.62, 135.49, 136.04, 139.38, 146.34, 158.36, 160.18, 166.08.

4.1.3.11. 2-[(6-chloro-4-oxo-3-phenyl-3,4-dihydroquinazoline-2-yl)thio]-N-(4-chlorophenyl)acetamide. ***(29)***. 2-[(6-chloro-4-oxo-3-phenyl-3,4-dihydroquinazoline-2-yl)thio]-*N*-(4-chlorophenyl)acetamide. **(29).** white solid (yield 88.65%). m.p. 230 °C; IR (KBr, cm^{-1}): 3282 (NH), 3059 (C—H aromatic), 2985 (C—H aliphatic), 1697 (CO amide), 1654 (CO amide) and 1543 (amide II band); ^{1}H NMR (DMSO-d_6, 400 MHz) δ (ppm): 4.08 (s, 2H, CH_2CO), 7.36 (d, *J* = 8.80 *Hz*, 2H, Ar-H phenyl), 7.51

(dd, $J = 7.10, 2.50$ *Hz*, 2H, Ar-H phenyl), 7.56 (t, $J = 8.70$ *Hz*, 1H, Ar-H phenyl), 7.61 (m, 4H, Ar-H phenyl), 7.64 (d, $J = 8.70$ *Hz*, 1H, Ar-H quinazoline), 7.86, (dd, $J = 8.70$ & 2.50 *Hz*, 1H, Ar-H quinazoline), 8.01 (d, $J = 2.40$ *Hz*, 1H, Ar-H quinazoline), 10.49 (s, 1H, D_2O exchangeable, NH). ^{13}C NMR (DMSO-d_6, 400 MHz) δ (ppm): 37.75, 121.15, 121.36, 126.00, 127.49, 128.55, 129.19, 129.78, 130.10, 130.51, 130.64, 135.49, 136.01, 138.33, 146.31, 158.29, 160.16, 166.33. Mass (*m/z*): 459 (M^++4), 457 (M^++2), 455 (M^+), 449, 432, 431, 398, 386 (100%, base peak), 383, 340, 285, 279, 266, 263, 244, 222, 195, 193, 192, 130, 125, 101 and 71.

4.1.3.12. 2-[(6-chloro-4-oxo-3-phenyl-3,4-dihydroquinazoline-2-yl)thio]-N-(4-methoxyphenyl)acetamide. ***(30)***. 2-[(6-chloro-4-oxo-3-phenyl-3,4-dihydroquinazoline-2-yl)thio]-*N*-(4-methoxyphenyl)acetamide. **(30).** white solid (yield 83.35%). m.p. 200 °C; IR (KBr, cm^{-1}): 3302 (NH), 3055 (C—H aromatic), 2978 & 2916 (C—H aliphatic), 1701 (CO amide), 1651 (CO amide) and 1540 (amide II band); ^{1}H NMR (DMSO-d_6, 400 MHz) δ (ppm): 3.72 (s, 3H, OCH_3), 4.06 (s, 2H, CH_2CO), 6.87 (d, $J = 9.00$ *Hz*, 2H, Ar-H phenyl), 7.50 (m, 4H, Ar-H phenyl), 7.60 (m, 4H, Ar-H), 7.86, (dd, $J = 8.70$ & 2.50 *Hz*, 1H, Ar-H quinazoline), 8.02 (d, $J = 2.40$ *Hz*, 1H, Ar-H quinazoline), 10.20 (s, 1H, D_2O exchangeable, NH). ^{13}C NMR (DMSO-d_6, 400 MHz) δ (ppm): 37.72, 55.63, 114.37, 121.19, 121.36, 125.99, 128.60, 129.79, 130.08, 130.48, 130.61, 132.50, 135.49, 136.04, 146.36, 155.83, 158.38, 160.19, 165.53.

4.1.3.13. 2-[(3-Ethyl-6-nitro-4-oxo-3,4-dihydroquinazoline-2-yl)thio]-N-phenylacetamide. ***(31)***. 2-[(3-Ethyl-6-nitro-4-oxo-3,4-dihydroquinazoline-2-yl)thio]-*N*-phenylacetamide. **(31).** yellow solid (yield 88.15%). m.p. 205 °C; IR (KBr, cm^{-1}): 3356 (NH), 3062 (C—H aromatic), 2978 & 2939 (C—H aliphatic), 1678 (CO amide) and 1539 & 1338 (NO_2); ^{1}H NMR (DMSO-d_6, 400 MHz) δ (ppm): 1.34 (t, $J = 7.00$ *Hz*, 3H, CH_3CH_2), 4.16 (q, $J = 6.90$ *Hz*, 2H, CH_3CH_2), 4.30 (s, 2H, CH_2CO), 7.07 (t, $J = 7.30$ *Hz*, 1H, Ar-H phenyl), 7.33 (dd, $J = 7.80$ & 7.30 *Hz*, 2H, Ar-H phenyl), 7.61 (m, 3H, Ar-H), 8.51 (dd, $J = 9.00$ & 2.70 *Hz*, 1H, Ar-H quinazoline), 8.76 (d, $J = 2.60$ *Hz*, 1H, Ar-H quinazoline), 10.45 (s, 1H, D_2O exchangeable, NH). ^{13}C NMR (DMSO-d_6, 400 MHz) δ (ppm): 13.09, 37.42, 119.22, 119.71, 123.27, 124.02, 127.83, 129.27, 129.30, 139.35, 144.55, 150.92, 159.94, 161.36, 165.86.

4.1.3.14. 2-[(6-nitro-4-oxo-3-phenyl-3,4-dihydroquinazoline-2-yl)thio]-N-phenylacetamide. ***(32)***. 2-[(6-nitro-4-oxo-3-phenyl-3,4-dihydroquinazoline-2-yl)thio]-*N*-phenylacetamide. **(32).** white solid (yield 88.60%). m.p. 230 °C; IR (KBr, cm^{-1}): 3352 (NH), 3093 & 3059 (C—H aromatic), 1693 (CO amide), 1681 (CO amide) and 1539 & 1338 (NO_2); ^{1}H NMR (DMSO-d_6, 400 MHz) δ (ppm): 4.15 (s, 2H, CH_2CO), 7.07 (t, $J = 7.40$ *Hz*, 1H, Ar-H phenyl), 7.52 (dd, $J = 7.90$ & 7.40 *Hz*, 2H, Ar-H phenyl), 7.61 (m, 6H, Ar-H), 7.72 (d, $J = 9.00$ *Hz*, 1H, Ar-H phenyl), 7.87 (t, $J = 8.80$ *Hz*, 1H, Ar-H quinazoline), 8.59 (dd, $J = 9.00$ & 2.70 *Hz*, 1H, Ar-H quinazoline), 8.77 (d, $J = 2.60$ *Hz*, 1H, Ar-H quinazoline), 10.38 (s, 1H, D_2O exchangeable, NH). ^{13}C NMR (DMSO-d_6, 400 MHz) δ (ppm): 39.41, 119.75, 120.12, 123.15, 124.14, 128.54, 129.09, 129.32, 129.58, 130.27, 130.62, 135.63, 139.04, 144.62, 145.34, 152.14, 161.06, 163.18.

4.1.3.15. N'-{2-[(3-Ethyl-7-nitro-4-oxo-3,4-dihydroquinazoline-2-yl)thio]acetyl}benzohydrazide. ***(33)***. *N'*-{2-[(3-Ethyl-7-nitro-4-oxo-3,4-dihydroquinazoline-2-yl)thio]acetyl}benzohydrazide. **(33).** white solid (yield 87.30%). m.p. 235 °C; IR (KBr, cm^{-1}): 3182 (NH), 3024 (C—H aromatic), 2993 & 2943 (C—H aliphatic), 1681 (CO amide), 1554 (amide II band) and 1535 & 1342 (NO_2); ^{1}H NMR (DMSO-d_6, 400 MHz) δ (ppm): 1.33 (t, $J = 6.68$ *Hz*, 3H, CH_3CH_2), 4.14 (q, $J = 6.84$ *Hz*, 2H, CH_3CH_2), 4.21 (s, 2H, CH_2CO), 7.49 (dd, $J = 7.32$ & 7.04 *Hz*, 2H, Ar-H phenyl), 7.57 (t, $J = 6.88$ *Hz*, 1H, Ar-H phenyl), 7.87 (d, $J = 7.44$ *Hz*, 2H, Ar-H phenyl), 8.16 (d, $J = 8.56$ *Hz*, 1H, Ar-H quinazoline), 8.29 (d, $J = 8.76$ *Hz*, 1H, Ar-H quinazoline), 8.53 (s, 1H, Ar-H quinazoline), 10.48 (s, 1H, D_2O exchangeable, NH), 10.51 (s, 1H, D_2O exchangeable, NH). ^{13}C NMR (DMSO-d_6, 400 MHz) δ (ppm): 13.16, 34.46, 40.39, 119.86, 122.02, 123.45, 127.92, 128.93, 129.04, 132.35, 132.78, 147.45, 151.64, 158.93, 159.88, 165.94, 166.79.

4.1.3.16. N'-{2-[(6-Chloro-3-ethyl-4-oxo-3,4-dihydroquinazoline-2-yl)thio]acetyl}benzohydrazide. ***(34)***. *N'*-{2-[(6-Chloro-3-ethyl-4-oxo-3,4-dihydroquinazoline-2-yl)thio]acetyl}benzohydrazide. **(34).** brown solid (yield 83.80%). m.p. 175 °C; IR (KBr, cm^{-1}): 3194 (NH), 3070 & 3028 (C—H aromatic), 2981 & 2935 (C—H aliphatic), 1690 (CO amide), 1670 (CO amide) and 1546 (amide II band); ^{1}H NMR (DMSO-d_6, 400 MHz) δ (ppm): 1.31 (t, $J = 7.00$ *Hz*, 3H, CH_3CH_2), 4.11 (q, $J = 7.00$ *Hz*, 2H, CH_3CH_2), 4.16 (s, 2H, CH_2CO), 7.50 (d, $J = 7.50$ *Hz*, 2H, Ar-H phenyl), 7.58 (t, $J = 7.50$ *Hz*, 1H, Ar-H phenyl), 7.71 (d, $J = 8.70$ *Hz*, 1H, Ar-H quinazoline), 7.87 (m, 3H, Ar-H), 8.02 (d, $J = 2.40$ *Hz*, 1H, Ar-H quinazoline), 10.40 (s, 1H, D_2O exchangeable, NH), 10.50 (s, 1H, D_2O exchangeable, NH). ^{13}C NMR (DMSO-d_6, 400 MHz) δ (ppm): 12.29, 13.35, 34.38, 120.48, 125.64, 127.94, 128.92, 129.04, 130.47, 132.32, 132.83, 135.13, 145.95, 156.74, 159.85, 165.86, 166.69.

4.1.3.17. N'-{2-[(6-Chloro-4-oxo-3-phenyl-3,4-dihydroquinazoline-2-yl)thio]acetyl}benzohydrazide. ***(35)***. *N'*-{2-[(6-Chloro-4-oxo-3-phenyl-3,4-dihydroquinazoline-2-yl)thio]acetyl}benzohydrazide. **(35).** White solid (yield 78.20%). m.p. 200 °C; IR (KBr, cm^{-1}): 3194 (NH), 3066 & 3032 (C—H aromatic), 2978 (C—H aliphatic), 1693 (CO amide) and 1546 (amide II band); ^{1}H NMR (DMSO-d_6, 400 MHz) δ (ppm): 4.03 (s, 2H, CH_2CO), 7.47 (m, 4H, Ar-H phenyl), 7.60 (m, 4H, Ar-H phenyl), 7.78 (d, $J = 8.70$ *Hz*, 1H, Ar-H quinazoline), 7.85 (d, $J = 7.40$ *Hz*, 2H, Ar-H phenyl), 7.91 (dd, $J = 8.70$ & 2.50 *Hz*, 1H, Ar-H quinazoline), 8.03 (d, $J = 2.40$ *Hz*, 1H, Ar-H quinazoline), 10.40 (s, 1H, D_2O exchangeable, NH), 10.50 (s, 1H, D_2O exchangeable, NH). ^{13}C NMR (DMSO-d_6, 400 MHz) δ (ppm): 34.92, 121.31, 125.86, 127.92, 128.93, 129.13, 129.79, 130.11, 130.57, 130.66, 132.32, 132.81, 135.40, 135.95, 146.39, 157.84, 160.25, 165.84, 166.68.

4.1.3.18. N'-{2-[(3-Ethyl-6-nitro-4-oxo-3,4-dihydroquinazoline-2-yl)thio]acetyl}benzohydrazide. ***(36)***. *N'*-{2-[(3-Ethyl-6-nitro-4-oxo-3,4-dihydroquinazoline-2-yl)thio]acetyl}benzohydrazide. **(36).** brown solid (yield 83.50%). m.p. 165 °C; IR (KBr, cm^{-1}): 3201 (NH), 3035 (C—H aromatic), 2989 & 2947 (C—H aliphatic), 1693 (CO amide), 1516 (amide II band) and 1546, 1342 (NO_2); ^{1}H NMR (DMSO-d_6, 400 MHz) δ (ppm): 1.34 (t, $J = 7.00$ *Hz*, 3H, CH_3CH_2), 4.16 (q, $J = 6.80$ *Hz*, 2H, CH_3CH_2), 4.23 (s, 2H, CH_2CO), 7.50 (dd, $J = 7.50$ & 7.20 *Hz*, 2H, Ar-H phenyl), 7.58 (t, $J = 7.20$ *Hz*, 1H, Ar-H phenyl), 7.87 (m, 3H, Ar-H), 8.56 (dd, $J = 9.00$ & 2.60 *Hz*, 1H, Ar-H quinazoline), 8.78 (d, $J = 2.60$ *Hz*, 1H, Ar-H quinazoline), 10.44 (s, 1H, D_2O exchangeable, NH), 10.52 (s, 1H, D_2O exchangeable, NH). ^{13}C NMR (DMSO-d_6, 400 MHz) δ (ppm): 13.03, 34.51, 40.48, 119.05, 123.07, 127.89, 128.46, 128.99, 129.02, 132.47, 132.61, 144.56, 150.92, 160.06, 160.79, 166.20, 166.73.

4.1.3.19. N'-{2-[(6-nitro-4-oxo-3-phenyl-3,4-dihydroquinazoline-2-yl)thio]acetyl}benzohydrazide. ***(37)***. *N'*-{2-[(6-nitro-4-oxo-3-phenyl-3,4-dihydroquinazoline-2-yl)thio]acetyl}benzohydrazide. **(37).** brown solid (yield 84.00%). m.p. 190 °C; IR (KBr, cm^{-1}): 3240 (NH), 3062 & 3035 (C—H aromatic), 2889 (C—H aliphatic), 1697 (CO amide), 1519 (amide II band) and 1546, 1338 (NO_2); ^{1}H NMR (DMSO-d_6, 400 MHz) δ (ppm): 4.09 (s, 2H, CH_2CO), 7.50 (m, 5H, Ar-H phenyl), 7.60 (m, 3H, Ar-H phenyl), 7.86 (dd, $J = 7.50$ *Hz*, 2H, Ar-H phenyl), 7.93 (d, $J = 9.00$ *Hz*, 1H, Ar-H quinazoline), 8.63 (dd, $J = 9.00$ & 2.60 *Hz*, 1H, Ar-H quinazoline), 8.79 (d, $J = 2.50$ *Hz*, 1H, Ar-H quinazoline), 10.38 (s, 1H, D_2O exchangeable, NH), 10.48 (s, 1H, D_2O exchangeable, NH). ^{13}C NMR (DMSO-d_6, 400 MHz) δ (ppm): 35.14, 120.17, 123.18, 127.91, 128.54, 128.93, 129.39, 129.66, 130.24, 130.88, 132.34, 132.79, 135.66, 144.67, 151.51, 160.36, 162.05, 165.87, 166.51.

4.2. Biological testing

4.2.1. In vitro VEGFR-2 tyrosine kinase inhibitory assay

IC_{50} of all compounds against VEGFR-2 kinase were determined with enzyme linked immunosorbent assay (ELISA). Human VEGFR-2 ELISA kit was used. VEGFR-2 specific antibody was seeded on a 96 well microplate and 100 μL of solution of the standard or the tested compound was added. All were then incubated for 2.5 h. at room temperature then washed. 100 μL of prepared biotin antibody was then added and incubated at room temperature for 1 h then washed. 100 μL of streptavidin solution was then added and incubated at room temperature for 45 min. then washed. 100 μL of tetramethybenzidine (TMB) Substrate solution was added then incubated at room temperature for 30 min. Then 50 μL of the stop solution was added and immediately read at 450 nm. The standard curve was hence drawn, concentration was on the X-axis and the absorbance was on the Y-axis.

4.2.2. In vitro antiproliferative assay

Anti-proliferative activity screening was conducted against 3 human cancer cell lines namely; HepG2, PC3 and MCF-7. The cell lines were obtained from American Type Culture Collection (ATCC) via National Cancer Institute (Cairo, Egypt). All chemicals used in the assay were of high analytical grade and obtained from either Sigma-Alderich or Bio-rad. The antitumor activity was measured quantitatively and the assay was carried out according to MTT protocol [41]. This colorimetric assay is based on the conversion of the yellow tetrazolium bromide (MTT) to a purple formazan derivative by mitochondrial succinate dehydrogenase in viable cells. The cells were cultured in RPMI-1640 medium with 10% fetal bovine serum. Antibiotics added were 100 units/mL penicillin and 100 μg/mL streptomycin at 37C in a 5% CO_2 incubator. The cells were seeded in a 96-well plate at a density of $1.0x10^4$ cells/well. at 37C for 48 h under 5% CO_2. After incubation the cells were treated with different concentration of compounds and incubated for 24 h. After 24 h of drug treatment, 20 μL of MTT solution at 5 mg/ml was added and incubated for 4 h. Dimethyl sulfoxide (DMSO) in volume of 100 μL is added into each well to dissolve the purple formazan formed. The colorimetric assay is measured and recorded at absorbance of 570 nm using a plate reader (EXL 800, USA). The relative cell viability in percentage was calculated as (A570 of treated samples/A570 of untreated sample) X 100.

4.2.3. Selective cytotoxicity assay

In vitro antiproliferative assay against the normal human cell line WI-38 was carried out according to MTT protocol. The cell line was obtained from ATCC via National Cancer Institute (Cairo, Egypt).

4.2.4. Cell cycle analysis

In line with the protocol reported by Wang et al [42]. HepG2 cells were seeded and incubated in six-well plates for 24 h, each well contained 2×10^5 cells. Fetal bovine serum (FBS, 10%) was then added and the cells were incubated at 37 °C and 5% CO2. The medium was then replaced with DMSO (1% v/v) containing the 4.6 μM of compound **36** and incubated for 48 h then washed with cold phosphate buffered saline (PBS), fixed with 70% ethyl alcohol, rinsed with PBS then stained with the DNA fluorochrome propidium iodide (PI) then kept for 15 min at 37 °C. The samples were hence analyzed with a FACS Caliber flow cytometer.

4.2.5. Apoptosis assay

Annexin V fluorescein isothiocyanate (V-FITC)/PI kit was used for apoptosis detection according to the reported method [43].

4.3. In silico studies

4.3.1. Molecular modeling

The molecular modeling study was performed using the Molecular Operating Environment (MOE 2010) software. The three-dimensional structures and conformations of the enzymes were acquired from the Protein Data Bank (PDB) website using VEGFR-2 complexed with pyrrolopyrimidine inhibitor (PDB code 3VHE). The ligand molecules were constructed in MOE using the builder module and collected in a database. The database was prepared by using the option "Protonate 3D" to add hydrogens, calculate partial charges and minimize energy (using Force Field MMFF94x). In addition, the protein structure was prepared by deleting the repeated chains, water molecules and any surfactants, hydrogens were also added to the atom of the receptor and the partial charges were calculated. MOE was used to calculate the best score between the ligands and the enzymes' binding sites. Scoring was determined using alpha HB as a scoring function. The resulted database contained the score between the ligands' conformers and the enzyme binding sites in kcal/mol. To confirm the credibility of docking results, self-docking was used to validate the adopted docking protocol in which co-crystallized ligand were drawn in MOE, prepared as the targeted compounds (hydrogens addition, partial charges calculation and energy minimization), and then docked into the active site of the protein using the same protocol. The top ranked pose exhibited Root mean square deviation (RMSD) value of less than 0.42 Å from the experimental crystal structure. This result indicated that the Molecular Operating Environment (MOE) docking could reliably predict docking pose for the studied compounds to an enzyme. It was reported that values less than 1.5 or 2 Å were a sign of a successful and reliable docking protocol.

4.3.2. In silico ADMET analysis

ADMET descriptors (absorption, distribution, metabolism, excretion and toxicity) of the synthesized compounds were determined using Discovery studio 4.0. At first, the CHARMM force field was applied then the compounds were prepared and minimized according to the preparation of small molecule protocol. Then ADMET descriptors protocol was applied to carry out these studies [44].

Declaration of Competing Interest

The authors declare that they have no known competing financial interests or personal relationships that could have appeared to influence the work reported in this paper.

Appendix A. Supplementary material

Supplementary data to this article can be found online at https://doi.org/10.1016/j.bioorg.2021.104695.

References

[1] R.L. Siegel, K.D. Miller, A. Jemal, Cancer statistics, 2020, CA. Cancer J. Clin. (2020), https://doi.org/10.3322/caac.21590.
[2] A. Hoeben, B. Landuyt, M.S. Highley, H. Wildiers, A.T. Van Oosterom, E.A. De Bruijn, Vascular endothelial growth factor and angiogenesis, Pharmacol. Rev. (2004), https://doi.org/10.1124/pr.56.4.3.
[3] L.A. Sullivan, R.A. Brekken, The VEGF family in cancer and antibody-based strategies for their inhibition, MAbs (2010), https://doi.org/10.4161/mabs.2.2.11360.
[4] N. Ferrara, R.S. Kerbel, Angiogenesis as a therapeutic target, Nature (2005), https://doi.org/10.1038/nature04483.
[5] L. Shi, T.T. Wu, Z. Wang, J.Y. Xue, Y.G. Xu, Discovery of N-(2-phenyl-1H-benzo[d]imidazol-5-yl)quinolin-4-amine derivatives as novel VEGFR-2 kinase inhibitors, Eur. J. Med. Chem. (2014), https://doi.org/10.1016/j.ejmech.2014.07.071.
[6] A.K. Olsson, A. Dimberg, J. Kreuger, L. Claesson-Welsh, VEGF receptor signalling - In control of vascular function, Nat. Rev. Mol. Cell Biol. (2006), https://doi.org/10.1038/nrm1911.
[7] S. Guo, L.S. Colbert, M. Fuller, Y. Zhang, R.R. Gonzalez-Perez, Vascular endothelial growth factor receptor-2 in breast cancer, Biochim. Biophys. Acta - Rev. Cancer. (2010), https://doi.org/10.1016/j.bbcan.2010.04.004.
[8] N.R. Smith, D. Baker, N.H. James, K. Ratcliffe, M. Jenkins, S.E. Ashton, G. Sproat, R. Swann, N. Gray, A. Ryan, J.M. Jürgensmeier, C. Womack, Vascular endothelial growth factor receptors VEGFR-2 and VEGFR-3 are localized primarily to the vasculature in human primary solid cancers, Clin. Cancer Res. (2010), https://doi.org/10.1158/1078-0432.CCR-09-2797.

[9] S.E. Duff, M. Jeziorska, D.D. Rosa, S. Kumar, N. Haboubi, D. Sherlock, S. T. O'Dwyer, G.C. Jayson, Vascular endothelial growth factors and receptors in colorectal cancer: Implications for anti-angiogenic therapy, Eur. J. Cancer. (2006), https://doi.org/10.1016/j.ejca.2005.09.018.

[10] S. Ghosh, C.A.W. Sullivan, M.P. Zerkowski, A.M. Molinaro, D.L. Rimm, R.L. Camp, G.G. Chung, High levels of vascular endothelial growth factor and its receptors (VEGFR-1, VEGFR-2, neuropilin-1) are associated with worse outcome in breast cancer, Hum. Pathol. (2008), https://doi.org/10.1016/j.humpath.2008.06.004.

[11] T. Seto, M. Higashiyama, H. Funai, F. Imamura, K. Uematsu, N. Seki, K. Eguchi, T. Yamanaka, Y. Ichinose, Prognostic value of expression of vascular endothelial growth factor and its flt-1 and KDR receptors in stage I non-small-cell lung cancer, Lung Cancer. (2006), https://doi.org/10.1016/j.lungcan.2006.02.009.

[12] G. Xia, S.R. Kumar, D. Hawes, J. Cai, L. Hassanieh, S. Groshen, S. Zhu, R. Masood, D.I. Quinn, D. Broek, J.P. Stein, P.S. Gill, Expression and significance of vascular endothelial growth factor receptor 2 in bladder cancer, J. Urol. (2006), https://doi.org/10.1016/S0022-5347(05)00736-6.

[13] P.A. Harris, A. Boloor, M. Cheung, R. Kumar, R.M. Crosby, R.G. Davis-Ward, A. H. Epperly, K.W. Hinkle, R.N. Hunter, J.H. Johnson, V.B. Knick, C.P. Laudeman, D. K. Luttrell, R.A. Mook, R.T. Nolte, S.K. Rudolph, J.R. Szewczyk, A.T. Truesdale, J. M. Veal, L. Wang, J.A. Stafford, Discovery of 5-[[4-[(2,3-dimethyl-2H-indazol-6-yl) methylamino]-2- pyrimidinyl]amino]-2-methyl-benzenesulfonamide (pazopanib), a novel and potent vascular endothelial growth factor receptor inhibitor, J. Med. Chem. (2008), https://doi.org/10.1021/jm800566m.

[14] D. Strumberg, M.E. Scheulen, B. Schultheis, H. Richly, A. Frost, M. Büchert, O. Christensen, M. Jeffers, R. Heinig, O. Boix, K. Mross, Regorafenib (BAY 73–4506) in advanced colorectal cancer: A phase I study, Br. J. Cancer. (2012), https://doi.org/10.1038/bjc.2012.153.

[15] M.J. Ratain, T. Eisen, W.M. Stadler, K.T. Flaherty, S.B. Kaye, G.L. Rosner, M. Gore, A.A. Desai, A. Patnaik, H.Q. Xiong, E. Rowinsky, J.L. Abbruzzese, C. Xia, R. Simantov, B. Schwartz, P.J. O'Dwyer, Phase II placebo-controlled randomized discontinuation trial of sorafenib in patients with metastatic renal cell carcinoma, J. Clin. Oncol. (2006), https://doi.org/10.1200/JCO.2005.03.6723.

[16] S. Wilhelm, C. Carter, M. Lynch, T. Lowinger, J. Dumas, R.A. Smith, B. Schwartz, R. Simantov, S. Kelley, Discovery and development of sorafenib: A multikinase inhibitor for treating cancer, Nat. Rev. Drug Discov. (2006), https://doi.org/10.1038/nrd2130.

[17] L.J. Kong, H. Li, Y.J. Du, F.H. Pei, Y. Hu, L.L. Zhao, J. Chen, Vatalanib, a tyrosine kinase inhibitor, decreases hepatic fbrosis and sinusoidal capillarization in CCl4-induced fbrotic mice, Mol. Med. Rep. (2017), https://doi.org/10.3892/mmr.2017.6325.

[18] S.J. Modi, V.M. Kulkarni, Vascular Endothelial Growth Factor Receptor (VEGFR-2)/KDR Inhibitors: Medicinal Chemistry Perspective, Med. Drug Discov. (2019), https://doi.org/10.1016/j.medidd.2019.100009.

[19] F. Zuccotto, E. Ardini, E. Casale, M. Angiolini, Through the "gatekeeper door": Exploiting the active kinase conformation, J. Med. Chem. (2010), https://doi.org/10.1021/jm901443h.

[20] L. Lintnerová, M. García-Caballero, F. Gregáň, M. Melicherčík, A.R. Quesada, J. Dobiaš, J. Lác, M. Sališová, A. Boháč, A development of chimeric VEGFR2 TK inhibitor based on two ligand conformers from PDB: 1Y6A complex - Medicinal chemistry consequences of a TKs analysis, Eur. J. Med. Chem. (2014), https://doi.org/10.1016/j.ejmech.2013.11.023.

[21] J. Blanc, R. Geney, C. Menet, Type II Kinase Inhibitors: An Opportunity in Cancer for Rational Design, Anticancer. Agents Med. Chem. (2013), https://doi.org/10.2174/1871520611313050008.

[22] J. Regan, C.A. Pargellis, P.F. Cirillo, T. Gilmore, E.R. Hickey, G.W. Peet, A. Proto, A. Swinamer, N. Moss, The kinetics of binding to p38 MAP kinase by analogues of BIRB 796, Bioorganic Med. Chem. Lett. (2003), https://doi.org/10.1016/S0960-894X(03)00656-5.

[23] L. Shi, T.T. Wu, Z. Wang, J.Y. Xue, Y.G. Xu, Discovery of quinazolin-4-amines bearing benzimidazole fragments as dual inhibitors of c-Met and VEGFR-2, Bioorganic Med. Chem. (2014), https://doi.org/10.1016/j.bmc.2014.07.008.

[24] L. Xi, J.Q. Zhang, Z.C. Liu, J.H. Zhang, J.F. Yan, Y. Jin, J. Lin, Novel 5-anilino-quinazoline-8-nitro derivatives as inhibitors of VEGFR-2 tyrosine kinase: Synthesis, biological evaluation and molecular docking, Org. Biomol. Chem. (2013), https://doi.org/10.1039/c3ob40368h.

[25] P.A. Plé, F. Jung, S. Ashton, L. Hennequin, R. Laine, R. Morgentin, G. Pasquet, S. Taylor, Discovery of AZD2932, a new Quinazoline Ether Inhibitor with high affinity for VEGFR-2 and PDGFR tyrosine kinases, Bioorganic Med. Chem. Lett. (2012), https://doi.org/10.1016/j.bmcl.2011.11.019.

[26] K. Lee, K.W. Jeong, Y. Lee, J.Y. Song, M.S. Kim, G.S. Lee, Y. Kim, Pharmacophore modeling and virtual screening studies for new VEGFR-2 kinase inhibitors, Eur. J. Med. Chem. (2010), https://doi.org/10.1016/j.ejmech.2010.09.002.

[27] Q.Q. Xie, H.Z. Xie, J.X. Ren, L.L. Li, S.Y. Yang, Pharmacophore modeling studies of type I and type II kinase inhibitors of Tie2, J. Mol. Graph. Model. (2009), https://doi.org/10.1016/j.jmgm.2008.11.008.

[28] M.A. Aziz, R.A.T. Serya, D.S. Lasheen, A.K. Abdel-Aziz, A. Esmat, A.M. Mansour, A. N.B. Singab, K.A.M. Abouzid, Discovery of Potent VEGFR-2 Inhibitors based on Furopyrimidine and Thienopyrimidne Scaffolds as Cancer Targeting Agents, Sci. Rep. (2016), https://doi.org/10.1038/srep24460.

[29] V.A. Machado, D. Peixoto, R. Costa, H.J.C. Froufe, R.C. Calhelha, R.M.V. Abreu, I. C.F.R. Ferreira, R. Soares, M.J.R.P. Queiroz, Synthesis, antiangiogenesis evaluation and molecular docking studies of 1-aryl-3-[(thieno[3,2-b]pyridin-7-ylthio)phenyl] ureas: Discovery of a new substitution pattern for type II VEGFR-2 Tyr kinase inhibitors, Bioorganic Med. Chem. (2015), https://doi.org/10.1016/j.bmc.2015.08.010.

[30] J. Dietrich, C. Hulme, L.H. Hurley, The design, synthesis, and evaluation of 8 hybrid DFG-out allosteric kinase inhibitors: A structural analysis of the binding interactions of Gleevec ®, Nexavar®, and BIRB-796, Bioorganic Med. Chem. (2010), https://doi.org/10.1016/j.bmc.2010.05.063.

[31] D.C.P. Singh, S.R. Hashim, R.G. Singhal, Synthesis and antimicrobial activity of some new thioether derivatives of quinoxaline, E-J. Chem. (2011), https://doi.org/10.1155/2011/482831.

[32] D. Kerzare, R. Chikhale, R. Bansode, N. Amnerkar, N. Karodia, A. Paradkar, P. Khedekar, Design, synthesis, pharmacological evaluation and molecular docking studies of substituted oxadiazolyl-2-oxoindolinylidene propane hydrazide derivatives, J. Braz. Chem. Soc. (2016), https://doi.org/10.5935/0103-5053.20160090.

[33] H.D. Gurupadaswamy, V. Girish, F. Zameer, R. Hegdekatte, J.B. Chauhan, S. A. Khanum, Synthesis of pyrimidones and evaluation of their xanthine oxidase inhibitory and antioxidant activities, Arch. Pharm. (Weinheim). (2013), https://doi.org/10.1002/ardp.201300240.

[34] A.A. Nasser, I.H. Eissa, M.R. Oun, M.A. El-Zahabi, M.S. Taghour, A. Belal, A. M. Saleh, A.B.M. Mehany, H. Luesch, A.E. Mostafa, W.M. Afifi, J.R. Rocca, H. A. Mahdy, Discovery of new pyrimidine-5-carbonitrile derivatives as anticancer agents targeting EGFRWTand EGFRT790M, Org. Biomol. Chem. (2020), https://doi.org/10.1039/d0ob01557a.

[35] H. van de Waterbeemd, E. Gifford, ADMET in silico modelling: towards prediction paradise?van de Waterbeemd, H., & Gifford, E. (2003). ADMET in silico modelling: towards prediction paradise? Nature Reviews. Drug Discovery, 2(3), 192–204. https://doi.org/10.1038/nrd1032, Nat. Rev. Drug Discov. (2003).

[36] T.I. Oprea, Section III Cheminformatics (in Drug Discovery), in: Oprea, T.I., Mannhold, R., Kubinyi, H. Folk. G. Eds., 2005. Chemoinformatics Drug Discov. Wiley-VCH., 2005.

[37] G. Klopman, L.R. Stefan, R.D. Saiakhov, ADME evaluation: 2. A computer model for the prediction of intestinal absorption in humans, Eur. J. Pharm. Sci. (2002), https://doi.org/10.1016/S0928-0987(02)00219-1.

[38] P.P. Roy, K. Roy, QSAR studies of CYP2D6 inhibitor aryloxypropanolamines using 2D and 3D descriptors, Chem. Biol. Drug Des. (2009), https://doi.org/10.1111/j.1747-0285.2009.00791.x.

[39] L. Yamini, K.M. Kumari, M. Vijjulatha, Molecular docking, 3D QSAR and designing of new quinazolinone analogues as DHFR inhibitors, Bull. Korean Chem. Soc. (2011), https://doi.org/10.5012/bkcs.2011.32.7.2433.

[40] M.A.A.-O., . S.T.A.-R., . H.I.E.-S., . S.G.A.H., Interaction of 2-thio-4-oxo-quinazoline Derivatives with Guinea Pig Liver Molybdenum Hydroxylases, Xanthine Oxidase and Aldehyde Oxidase, J. Biol. Sci. (2005). https://doi.org/10.3923/jbs.2005.370.378.

[41] D. Gerlier, N. Thomasset, Use of MTT colorimetric assay to measure cell activation, J. Immunol. Methods. (1986), https://doi.org/10.1016/0022-1759(86)90215-2.

[42] J. Wang, M.J. Lenardo, Roles of caspases in apoptosis, development, and cytokine maturation revealed by homozygous gene deficiencies, J. Cell Sci. (2000).

[43] K.K.W. Lo, T.K.M. Lee, J.S.Y. Lau, W.L. Poon, S.H. Cheng, Luminescent biological probes derived from ruthenium(II) estradiol polypyridine complexes, Inorg. Chem. (2008), https://doi.org/10.1021/ic701735q.

[44] M.K. Ibrahim, I.H. Eissa, A.E. Abdallah, A.M. Metwaly, M.M. Radwan, M. A. ElSohly, Design, synthesis, molecular modeling and anti-hyperglycemic evaluation of novel quinoxaline derivatives as potential PPARγ and SUR agonists, Bioorganic Med. Chem. (2017), https://doi.org/10.1016/j.bmc.2017.01.015.